AD

TECHNICAL REPORT ARBRL-TR-02084

M-82 PRIMER FLOW STUDY

Csaba K. Zoltani

June 1978

US ARMY ARMAMENT RESEARCH AND DEVELOPMENT COMMAND
BALLISTIC RESEARCH LABORATORY
ABERDEEN PROVING GROUND, MARYLAND

Destroy this report when it is no longer needed.
Do not return it to the originator.

Secondary distribution of this report by originating or sponsoring activity is prohibited.

Additional copies of this report may be obtained from the National Technical Information Service, U.S. Department of Commerce, Springfield, Virginia 22161.

The findings in this report are not to be construed as an official Department of the Army position, unless so designated by other authorized documents.

The use of trade names or manufacturers' names in this report does not constitute indorsement of any commercial product.

UNCLASSIFIED

SECURITY CLASSIFICATION OF THIS PAGE *(When Date Entered)*

REPORT DOCUMENTATION PAGE		READ INSTRUCTIONS BEFORE COMPLETING FORM
1. REPORT NUMBER TECHNICAL REPORT ARBRL-TR- 02084	2. GOVT ACCESSION NO.	3. RECIPIENT'S CATALOG NUMBER
4. TITLE *(and Subtitle)* M-82 PRIMER FLOW STUDY		5. TYPE OF REPORT & PERIOD COVERED Final 6. PERFORMING ORG. REPORT NUMBER
7. AUTHOR(s) Csaba K. Zoltani		8. CONTRACT OR GRANT NUMBER(s)
9. PERFORMING ORGANIZATION NAME AND ADDRESS US Army Ballistic Research Laboratory (ATTN: DRDAR-BLB) Aberdeen Proving Ground, MD 21005		10. PROGRAM ELEMENT, PROJECT, TASK AREA & WORK UNIT NUMBERS 1L1662617AH79
11. CONTROLLING OFFICE NAME AND ADDRESS US Army Armament Research and Development Command US Army Ballistic Research Laboratory (DRDAR-BL) Aberdeen Proving Ground, MD 21005		12. REPORT DATE JUNE 1978 13. NUMBER OF PAGES 73
14. MONITORING AGENCY NAME & ADDRESS *(if different from Controlling Office)*		15. SECURITY CLASS. *(of this report)* UNCLASSIFIED 15a. DECLASSIFICATION/DOWNGRADING SCHEDULE

16. DISTRIBUTION STATEMENT *(of this Report)*

Approved for public release; distribution unlimited.

17. DISTRIBUTION STATEMENT *(of the abstract entered in Block 20, if different from Report)*

18. SUPPLEMENTARY NOTES

19. KEY WORDS *(Continue on reverse side if necessary and identify by block number)*

Primer
Jet Flow
Gas Dynamics

20. ABSTRACT *(Continue on reverse side if necessary and identify by block number)*

This report describes a theoretical model and calculational results of the flow in an M-82 percussion primer from the time that the primer propellant is ignited up to 144 μs after the gases have exited the vent hole and enveloped an inert propellant charge in the chamber of a gun.

DD FORM 1 JAN 73 1473 EDITION OF 1 NOV 65 IS OBSOLETE

UNCLASSIFIED

SECURITY CLASSIFICATION OF THIS PAGE *(When Data Entered)*

TABLE OF CONTENTS

LIST OF FIGURES

LIST OF FIGURES

LIST OF FIGURES

I. INTRODUCTION

A quantitative description of the gas flow generated by a percussion primer is unavailable at the present time.* In this report we describe a theoretical model and calculational results of the flow in an M-82 percussion primer from the time that the primer propellant is ignited up to 144 μs after the gases have exited the vent hole and enveloped an inert propellant charge in the chamber of the gun.

The flow down the flash tube from the primer combustion chamber has been modeled as one-dimensional, time-dependent flow using the RECRIF code.[1] The gas motion into the gun chamber, in turn, was obtained from the revised SAMS code.[2] Outside of the primer combustion chamber the flow has been treated as that of a single-phase, non-reactive medium.

In Chapter II, we describe the flow model, the mathematical aspects of the simulation and experimental observations used in the validation of the results. The next chapter discusses the results of the calculations while in the last section we draw general conclusions about the results.

II. THE FLOW MODEL

A. The Physical Model

1. Overview

The M-82 percussion primer consist of 22 grains (1.43×10^{-3} kg) of slow burning class 3 black powder occupying a volume of 1.528×10^{-6} (m^3) of the forward end of the primer combustion chamber. The web size of the propellant was taken as 1.2×10^{-3} (m). The rest of the chamber is filled with an inert material. The combustion chamber is connected by a flash tube of 1.24×10^{-1} (m) in length and 6.3×10^{-3} (m) in diameter through an opening, called the vent hole, to the chamber housing the propellant bags (Figure 1).†

---

* An understanding of the dynamical processes at the primer charge interface is of interest to charge designers in their effort to achieve smooth pressure transient in new charge configurations.

[1] Celmins, A. K. R., "RECRIF Users' Manual", BRL MR 2693, October 1976.

[2] Farr, J. L. and Traci, R. M., "A Users' Manual for SAMS", BRL Contract Report 162, June 1974.

† See Appendix for figures.

Upon ignition, the pressure in the primer chamber increases. A pressure wave, followed by the combustion products of the propellant which consist of burnt gas, unburnt propellant grains and solid products of combustion, moves down the tube, finally exiting at the vent hole. To prevent the propellant grains from blowing out of the combustion chamber, a blowout disc, 1.0×10^{-3} (kg) in mass, is located at the entrance of the flash tube at time t = 0. The hold-back pressure of the disc was set at 2.07×10^{7} (Pa) ensuring a pressure buildup in the combustion chamber prior to the disc motion. The bore resistance of the flash tube was assumed to be 1.67×10^{2} (N) and the friction coefficient assumed to be 5.0×10^{-3}.

The vent hole conditions, after a short transient, correspond to that of choked flow leading to an underexpanded jet in the chamber housing the propellant bags.

With a stand-off, that is a space between the vent hole and the propellant bag, as in the present study, the gas upon exiting the flash tube expands. The flow is preceded by a weak shock which impinges upon and is reflected from the base of the propellant bag. The gas in turn, due to the geometrical constraints and in view of the pressure gradients present, flows along and around the propellant bag, eventually completely enveloping it.

In this study, the vent hole at the opening was 6.35×10^{-3} (m) in diameter, the stand-off 5.08×10^{-2} (m), the gun tube chamber 17.78×10^{-2} (m) in diameter and the spacing between the symmetrically placed propellant bag and the gun tube wall was 0.63×10^{-2} (m).

The propelling charge of the round consists of bags of propellant grains, rather closely packed, with typically a center core ignitor. The breech end of the bag is terminated by a pad of black powder which is ignited by the hot gases of the primer, thus ultimately leading to the ignition of the whole charge. By this time the propellant bag breaks up, the propellant grains fill the whole chamber, resulting in a fluidized mixture of propellant and combustion gases. With the increase in pressure, the bore resistance is overcome, the projectile starts to accelerate down the tube, enlarging the chamber volume available for combustion and ultimately, when the increase in volume is no longer compensated by the rate of gas generation, a decrease in chamber pressure can be observed.

An accurate tailoring of the heat and mass source represented by the primer is then essential for a smooth ignition of the propelling charge of the gun.

2. Flow Through the Initiator

Upon initiation, the combustion of the primer grains generates a mass of high pressure gases. These gases flow down a duct, called the flash tube, exiting into the chamber holding the propellant bags. For purposes of this simulation, it was assumed that the combustion chamber of the primer is connected by a constant area tube, terminating at the vent tube to the stand-off region. Thus, wave reflection due to changes in geometry is neglected. Only product gases were allowed to exit the combustion chamber and the blow out disc, after it reaches the vent hole, is automatically removed from the system, i.e., no longer considered as an influence on the flow development.

The flow in the flash tube is assumed to be one-dimensional, laminar, compressible, inviscid, and time-dependent; and chemical reactions are assumed to be completed by the time they exit the primer combustion chamber. The details of the chemical kinetics in the flow are not known at the present time, but by using a high enthalpy gas, with a temperature in the combustion chamber corresponding to that of the flame temperature of the propellant, a good approximation of the flow is obtained. The Noble-Abel equation of state, with the co-volume taken as zero was used in the calculations. In Table I, the pertinent geometrical and propellant parameters of the M-82 primer are listed.

Table I. M-82 Primer Characteristics

Geometry	
Volume occupied by the Class 3 Black Powder	1.528×10^{-6} (m^3)
Flash Tube Diameter	6.3×10^{-3} (m)
Flash Tube Exit Diameter	0.635×10^{-2} (m)
Flash Tube Length	0.124 (m)
Combustion Chamber Volume	9.310×10^{-6} (m^3)
Propellant (Class 3 Black Powder)	
Mass	1.43×10^{-3} (kg)
Burning Rate Exponent	7.540×10^{-1}
Burning Rate Coefficient	6.110×10^{-7}
Ratio of Specific Heats	1.20
Web Size	0.0012 (m)
Explosive Force	2.800×10^{4} (m)
Flame Temperature	2.030×10^{3} (K)

To account for the presence of particles in the flow without the benefit of a multiphase analysis, both the molecular weight and the ratio of specific heats have to be adjusted. The degree of modification needed depends on the mass of the suspended particles. For low particle loading satisfactory flow predictions based on a one-phase model may be obtained.

Particle laden flows have been studied intensely in connection with the rocket program where considerable degradation of nozzle performance was observed.[3] In these studies, particles represented up to 30% of the total mass flow. Only rudimentary studies of gas particle jets exist. Two-phase jets have been treated as gas jets with an increased density. For a particle jet to be dynamically equivalent to a gas jet the gas jet must have not only the same average density, but must also exhibit the same mass and momentum flux. Injected particles generally have to travel considerable distances before they reach the gas velocity, and, as Rudinger[3] has shown, for most practical cases, this is an unlikely event.

Neglecting the effect of turbulence, assuming uniform distribution of the particles over the cross section of the duct, uniformity in size and physical properties, precluding evaporation, condensation, chemical reaction or breakup of the particles and with particle size of the order of 1 μm, the analysis is straightforward.

Within the context of a one-phase flow analysis, one can account for some two-phase flow effects, such as the decrease of the specific heat ratio, with an increase in mass fraction of the mixture.

For mass fractions as low as 0.03 and a density ratio of

$$\frac{\varrho}{\rho_p} \sim 0(10^{-3}),$$

such as in the present case, the particles can be looked upon as a species of heavy molecules, with a molecular weight that is several orders of magnitude larger than the gas. In effect, one assumes then that the contribution of the particles to the pressure is negligible. The equation of state for the mixture then follows from the perfect gas law but with the density of the mixture. As long as the particle volume can be neglected, a gas-particle mixture may be treated as a perfect gas with modified thermal properties.

[3]Rudinger, G., "Flow of Solid Particles in Gases", AGARDograph No. 222, AGARD, Neuilly Sur Seine, France, 1976.

Let σ_p = concentration of the particles and σ be the gas concentration. The mass fraction of the particles is given by $\phi = \frac{\sigma_p}{\sigma + \sigma_p}$, where the mixture density is $\rho_m = \sigma + \sigma_p$.

One can now derive a relationship for the equation giving the ratio of specific heats for the gas particle mixture. Following Rudinger[3,4,5] the internal energy of the mixture can be expressed as

$$e_m = (1-\phi)c_v T + \phi c\tau$$

where $(1-\phi)$ represents the mass of the gas and τ is the temperature of the particles and ϕ is the particle mass fraction. The enthalpy can then be written as

$$h_m = e_m + \frac{p}{\rho_m} = (1-\phi)\ c_v T + \phi c\ \tau + \frac{p}{\rho_m}$$

Recalling the definitions of specific heat and substituting

$$c_{v_m} = \left(\frac{\partial e_m}{\partial T}\right)_v = (1-\phi)c_v + \phi c$$

$$c_{p_m} = \left(\frac{\partial h_m}{\partial T}\right)_p = (1-\phi)c_p + \phi c$$

consequently γ_m, the ratio of specific heats of the mixture is defined by

$$\gamma_m = \frac{(1-\phi)c_p + \phi c}{(1-\phi)c_v + \phi c}$$

or if γ = ratio of specific heats of the gas, $\delta = \frac{c}{c_p}$, where c is the specific heat of the solid particle and η the ratio of the mass of particles to the mass of the gas, then

---

[4]Rudinger, G., "Some Effects of Finite Particle Volume on the Dynamics of Gas Particle Mixtures", AIAA Journal 3, 1217-1222, (1965).

[5]Rudinger, G., "Relaxation in Gas-Particle Flow" in Nonequilibrium Flows, Part I, P. P. Wegener, Ed., Marcel Dekker, NY, 1969.

$$\gamma_m = \gamma \frac{1 + \eta\delta}{1 + \gamma\eta\delta} .$$

(Note that $\delta \approx O(1)$ for many gas particle combinations of interest).

There is considerable disagreement in the literature on the proper value for the specific heat of black powder. While the Encyclopedia of Explosives[6] give a value of $0.2\left[\frac{cal}{gm\text{-}deg}\right]$ calculations based on the actual composition of black powder, assuming 75% KNO_3, 15% charcoal and 10% sulphur yields a value of $c = 0.356\left[\frac{cal}{gm\text{-}deg}\right]$. This value is valid in the temperature range from 300 to 700[K]and represents an average value.

Using $\delta = 2.080$, $\eta = 0.03$, the value of γ_m turns out to be 1.22. At $\eta = 0.1$ (10% of the propellant unburnt) $\gamma_m = 1.192$. Thus, it was felt that $\gamma_m = 1.20$ was not an unreasonable value to use in the calculations.

For a calculation of the temperature of the product gases the molecular weight has to be known. If one assumes that the exhaust gases contain solid particles as products of combustion[7], which appears to be the case, the molecular weight is $61.6\left[\frac{kg}{kmol}\right]$. On the other hand, if a solid phase doesn't precipitate, the molecular weight turns out to be $35.0\left[\frac{kg}{kmol}\right]$. Based on the available evidence, we felt that the higher value is the more reasonable value to use in this simulation.

3. Flow at the Base of the Propellant Bag

The underexpanded jet formed at the vent hole spreads laterally and longitudinally, eventually contacting the base of the propellant bag, at which time the flow structure changes. A shock stands off the surface of the bag and a system of weak shocks may be observed as one goes radially along the propellant bag. The shock enables the flow to equilibrate with the ambient gas, given sufficient room for lateral expansion.

---

[6] Federoff, B. T. and Sheffield, O. E., "Encyclopedia of Explosives and Related Items", Volume 2. Picatinny Arsenal, Dover, NJ, 1962.

[7] Freedman, E., Private Communication.

In reality, due to the hole punched in the propellant bag by the primer jet, and the breakup of the bag, the flow is considerably more complicated, but neither experimental data nor a theoretical study of the process is available at the present time. For the case at hand, it was assumed that the bag retains its structural integrity; i.e., it does not move or burn and the primer flow may be treated analogously to a jet impinging normally onto a flat plate.

The jet was assumed to be an inviscid, one-component high-enthalpy but nonreactive gas. The confining surfaces, such as walls, for the purpose of this investigation were assumed to be inert and at ambient temperature. Also, a no-mass flux condition was strictly enforced on all surfaces.

In the stand-off space, for the calculations discussed in Chapter III, neither a Mach disk nor the stand-off shock could be detected. These are postulated in the classical theory for steady processes while the case at hand is unsteady. A quick calculation shows that if we assume steady conditions at the nozzle corresponding to that which prevails at $t = 0$, both the stand-off shock and the Mach disk would fall outside the physical region between the vent hole and the base of the inert bag. Thus, it appears fair to suppose that the flow will be subjected to a number of wave propagation processes and at no time will an equilibrium configuration be achieved.

According to observations of the impingement of non-uniform axisymmetric, supersonic, steady jets on a perpendicular flat plate in the Mach number regime $1.42 \leq M \leq 2.83$, a symmetrical shock, convex toward the nozzle, spans the jet.[8] The flow beneath the impingement shock is subsonic and is turned outward due to the plate. The streamlines are deflected outward and as the flow moves radially, a reacceleration with a sonic line near the jet edge can be observed. The constant pressure upper boundary of the wall jet region is the jet edge streamline which has undergone a centered expansion upon passing through the shock. Bubbles result from the interaction of the plate shock with very weak shock waves which are present in the flow.

The significance of these observations is that there are circumstances under which the point of maximum pressure does not occur on the stagnation streamline but rather off the center line. This pressure distribution has, as a consequence, the presence of a slowly recirculating fluid in the shock layer with the diameter of the bubble ranging up to 0.8 times the jet diameter. These flow anomalies may have some effect

---

[8] Kalghatgi, G. T., Hunt, B. L., "The Occurence of Stagnation Bubbles in Supersonic Jet Impingement Flows", Aeronautical Quarterly, 27, 169-185, 1976.

upon the site and distribution of the ignition spots on the propellant bag. In the present simulation only tenuous, circumstantial evidence for these mechanisms was observed. However, for primers with larger stand-off distances calculated by higher order techniques which introduce less smearing than present in this work, such shock phenomena may possibly be observed.

B. Mathematical Aspects of the Simulation

The calculation of the flow from the combustion chamber through the flash tube of the initiator-spindle assembly was based on the one-dimensional form of the conservation laws:

$$(\rho A)_t + (\rho u A)_x = 0$$

$$(\rho u A)_t + (u^2 \rho A)_x + A p_x + A \rho F = 0$$

$$[\rho A(e + \frac{1}{2} u^2)]_t + [\rho u A(e + \frac{1}{2} u^2) + \frac{p}{\rho}]_x - q\rho A = 0$$

and the Noble-Abel equation-of-state

$$p = \frac{R}{M} T \frac{\rho}{1-\eta\rho}$$

with η set equal to zero. These equations were put into characteristic form and solved numerically.[1]

Space-averaged values of the variables were used for the gas in the combustion chamber. The propellant obeyed the regression law

$$\frac{dz}{dt} = \beta p^n$$

where $z(t)$ represents the distance that the propellant has burnt, n, β are constants, and p is the pressure. With the assumption that the kinetic energy of the gas in the chamber is small compared to its internal energy, the average pressure can be approximated by the stagnation pressure. Thus, using an energy balance of the chamber with the burning rate equation and the continuity equation, all the flow variables can be computed.

The two-dimensional, time-dependent part of the calculation in the stand-off region was based on the Euler equations. The finite difference analog of the conservation laws was solved by a first-order, two-step algorithm which has been described elsewhere.[2] In the course of the

calculation, the shocks are captured and smeared over several cell widths, requiring fine gridding for the resolution of flow details in the vicinity of steep gradients.

A Noble-Abel equation-of-state was used with the co-volume set at $1.17 \times 10^{-3} [\frac{m^3}{kg}]$ which is valid for most of the commonly used propellants. Points along the solid boundaries were calculated by the reflection technique.

C. Experimental Observations

Only a limited amount of experimental data is available on the primer flow dynamics.[9,10,11] Pressure transducers along the chamber shaft of the initiator-spindle assembly, on the spindle, as well as on the test fixture and the breech end of the propellant bag, yield complete pressure time histories of the product gases (see Figure 1). Further, using high resolution photography, the expansion of the gases from the vent hole into the test fixture without a propellant bag have been observed (Figure 2). From these records the velocity of the gas cloud can be deduced and compared with calculational predictions. Some temperature measurements have also been attempted; but, at present, the observations are felt to be unreliable.[9,10] There is an urgent need for more experimental data on all facets of the primer flow dynamics.

Stiefel[9] reports that, for a gage located 0.0508 [m] from the axis of the tube and for an M-82 primer of the M-198 howitzer on the base of the propellant bag (P_3, Figure 1) with a stand-off of 0.025 [m], the height of the first pressure peak varied between 39 and 36 psi (2.68×10^5[Pa] and 2.48×10^5[Pa]), measured at 1.2 and 2.8 [ms] respectively for a straight-through duct. With a squared cone exit the pressure peaks, though of the same magnitude, were observed earlier, i.e., at 0.6 [ms]. However, in changing from a straight-through hole to a squared cone exit, the pressures exhibited more scatter; that is, they ranged between 33 and 44 psi (2.27×10^5[Pa] and 3.03×10^5[Pa]) in the experimental runs.

---

[9] Stiefel, L., "Experimental Characterization of the Output of Artillery Primers", (to be published).

[10] White, K. J., Hartman, R. A., May, I. W., Kelso, J. R., "Experimental Investigation of Ignition Train System for Bagged Charges", 14th JANNAF Combustion Meeting, (in press), 1977.

[11] White, J. J., Price, C. F., Holmes, H. E., May, I. W., "Black Powder and Clean Burning Ignitor Train Studies", 13th JANNAF Combustion Meeting, Vol. I, pp. 405-423, CPIA, Laurel, MD, 1976.

The experiments further showed that the velocity of the pressure wave is around 365 $[\frac{m}{s}]$ in the axial direction, while laterally, Stiefel[9] estimated a velocity of 40 $[\frac{m}{s}]$. White[10], based on time lapse photography of a primer jet exhausting into a chamber, found that the center core of the jet, at a distance of 0.1 [m] from the vent hole, propagates at 300 $[\frac{m}{s}]$.

III. RESULTS

A. Flash Tube Calculations

The calculational results can be divided into two parts: the flow in the flash tube between the primer combustion chamber and the vent hole and the flow in stand-off space between the vent hole and the propellant bag.

The one-dimensional calculations of the flow in the primer combustion chamber/flash tube were carried out using the RECRIF code. First, the burning rate exponent and coefficient were obtained from experimental data. These parameters and γ, the ratio of specific heats, were varied until the pressure-time behavior at the station 0.084[m] from the combustion chamber of the primer could be matched at the high end of the pressure-time curve (see Figure 3). A value of β of 6.10×10^{-7} with n, the burning rate exponent, equal to 0.754 and a $\gamma = 1.20$ gave acceptable results. The calculation of the flow over the whole length of the flash tube followed, with our primary interest centering on the vent hole conditions.

At $t = 5.00 \times 10^{-4}$[s] after the ignition of the black powder, the propellant gases reach the vent hole and, shortly afterwards, the flow is choked. In Figure 4 we have a plot of the mass of combustion products as a function of time in seconds. The uppermost curve gives the total mass burnt, while the lowest curve represents the propellant gas mass which has exited the flash tube. The difference in the ordinate for each time between the two lower curves gives the mass which is in the flash tube, while the difference between the two topmost curves gives the amount of mass still residing in the combustion chamber. Since we know the total propellant mass initially available, one can estimate the unburnt mass at each time. For example, if at $t = 1.514 \times 10^{-3}$[s] we assume that the unburnt particles are all evenly distributed within the flash tube and chamber, one arrives at a figure of 3% by mass of solid particles in the flow.

The velocity-time history of the flow in the flash tube is illustrated in Figure 5. The lower curve gives the velocity at the entrance to the flash tube from the primer combustion chamber while the other curve gives the velocity at the vent hole. This consists of two parts:

the rising portion gives the velocity of the blowout disc (i.e., the 1.0×10^{-3}[kg] plug which was used to prevent the unburnt particles from ejecting from the primer duct), while the decreasing portion gives the velocity at the muzzle. It should be noted that initially the flow is supersonic at the muzzle, but it drops continuously until sonic conditions are obtained. M = 1 occurs at the break in the slope of the curve.

The next two curves give the vent hole temperature, in degrees [K] and the vent hole pressure in [Pa] as a function of time [s]. Zero time refers to the inception of burning in the combustion chamber and the steep jump occurs as the flow reaches the vent hole. The break in the slope of the pressure curve again indicates transition to the choked condition.

From the data of the pressure, density and velocity at the vent hole, one obtains the following analytical expressions for these quantities as a function of time:

$$P = 0.128 \times 10^{14} \times t^2 - 0.302 \times 10^{11} \times t + 2.140 \times 10^{7}$$

$$\rho = 0.186 \times 10^{8} \times t^2 - 0.791 \times 10^{5} \times t + 9.141 \times 10$$

$$u = 0.802 \times 10^{8} \times t^2 - 1.451 \times 10^{5} \times t + 4.877 \times 10^{2}$$

The next four figures (8 through 11) give the velocity, temperature, pressure and density in the chamber and the flash tube at four different times, i.e., at $t = 3.733 \times 10^{-4}$, 7.466×10^{-4}, 1.120×10^{-3} and 1.493×10^{-3}[s]. The vertical line at the left is the separation point between the combustion chamber and the flash tube. The velocity appears as a linearly increasing function of distance while the temperature, except for the initial time, $t = 3.733 \times 10^{-4}$ [s], is a slowly decreasing function. It stays below the flame temperature since,as the gases expand, cooling takes place. This type behavior is as expected. The initial curve terminates at 5.9×10^{-2}[m], i.e., at the location of the blowout disc within the flash tube. At succeeding times in these figures, the disc has already exited the tube. The lower three curves terminate at the vent hole exit.

The gas velocity at the vent hole, as shown in Figure 8, is at a velocity of 420 $[\frac{m}{s}]$, but as time progresses and the pressure drops, it too drops. It is interesting to note the almost constant pressures and densities, at each time, all along the flash tube.

The conditions at the vent hole, which are the input conditions to the second phase of the calculations, that is the two-dimensional time-dependent flow in the stand-off zone, were followed for 1.514 [ms]. The pressure, velocity and density were then curve-fitted, using a Lagrangian interpolation technique, to give an analytical expression for the time behavior of these functions. The formulas were checked at various points along the time axis against the calculated values to insure the range of validity of the interpolation technique.

B. Flow in the Stand-off Region

Once the gases exit the vent hole, their behavior changes drastically. A one-dimensional analysis is no longer adequate as it is not able to account for the effect of the lateral motion in the space between the base pad and the vent hole. The computational results obtained by exercising the revised SAMS code will now be summarized.

With the time-dependent vent hole conditions as input, the initial runs calculated a free jet formed by the gas issuing from the flash tube. The results were then compared with the photographs shown in Figure 2(a) through 2(d).

Figures 12 and 13 show pressure contour plots of the jet with no charge in place at 23.14 and 66.19 [μs], respectively. The vent hole is located in the upper left-hand corner and the axis of the jet is at the left-hand border of the plot. At t = 23.14 [μs], for example, the pressure ratio across the plane of the vent hole is $\frac{p}{p_\infty} = 1.5$, resulting in an underexpanded jet. The closely spaced contour lines indicate the presence of a shock. As time progresses the shock weakens and also diffuses. This can be seen very clearly in the pressure-distance plot (along the jet axis) for the three different lines (Figure 14) where the pressure hump has spread and its amplitude lowered when the two curves are compared. The density plots, Figures 15 and 16, exhibit a behavior analogous to that of the pressure.

Along the spindle, in the vicinity of 2.0×10^{-2} [m] from the centerline of the jet, one sees a region of lower pressure, which is followed by a steep pressure rise as one approaches the blast wave.

The radial pressure distribution across the jet at three different times is shown in Figure 17, while near the tip of the jet, the pressure hump due to the blast wave is clearly discernible (Figure 18).

The velocity in the axial direction along the jet for t = 24.14, 45.73, and 66.19 [μs] is shown in Figure 19. Contrary to the contour plots, one should note that in this and the succeeding figures, the origin of the x-axis is at the vent hole and the coordinate increases in the downstream direction.

As the gas leaves the flash tube, the pressure ratio at the vent hole at the latter time is 1.06, so the conditions for an underexpanded jet are still clearly met. The gases expand and accelerate. A blast wave is seen to move with a peak velocity, at 66.19 [μs], of around 1500 $[\frac{m}{s}]$. The main body of the gas moves slower; near the center of the plume it is around 600 $[\frac{m}{s}]$.

From the photographs of Figure 2 one sees that the center of the plume propagates at around 300 $[\frac{m}{s}]$. This points out the main shortcoming of the present simulation. With a code which is restricted to a single γ for both the high enthalpy reaction products and the ambient, some of the calculated flow parameters will be inaccurate. We set the ambient density at the value corresponding to air at 300 [K] and, consequently, the ambient pressure, due to the γ used, becomes 0.485×10^5[Pa] instead of the 1.013×10^5[Pa]. Elementary shock wave theory then shows that the rate of shock propagation will be too high by a factor of a little over 2. On the other hand, the peak pressures, as shown below, can be calculated quite accurately.

With the propellant bag in place, modeled as a reflecting wall at 0.025[m] from the vent hole, the jet cannot proceed far downstream before it is turned radially. The pressure contour plots, Figures 20 and 21, give an overall view of the development of the flow. Again, at the edge of the plume a strong blast is in evidence which weakens as it moves away from the jet axis. A region of low pressure behind the blast is in evidence in Figure 20b and even more clearly in Figure 21. At t = 144.40 [μs], near the end of the simulation, the blast wave has weakened to the point where the pressure ratio at the head of the wave, with respect to the conditions ahead of it, is less than 3. The density contour plots, Figures 22 and 23, mimic those of the pressure.

Considerable computational information is avaiable for the pressure distribution within the flow field and comparison with experimental data is possible. Along the jet axis (Figures 24 through 26, from the vent hole to the propellant bag, the pressure is decreasing from an initial value of 1.6×10^7[Pa] at t = 74.73[μs], for example, at the vent hole, to 1.05×10^5[Pa] at the stagnation point. Over the time range of this calculation, as the vent hole pressure changed only marginally from 2.14×10^7[Pa] to 1.5×10^7[Pa] at t = 144.40[μs], quasi-steady conditions were observed at the propellant bag. After the initial transient, the pressure at the stagnation point changed by less than 11% so that conditions there corresponded to a quasi-steady state. This is no longer true as one proceeds radially along the base of the propellant bag. In Figure 27 one can clearly see the blast wave sweeping the surface. The flow is expanding behind the wave with the pressure

continuously dropping. At t = 46.44[μs] in Figure 27, the lowest pressure behind the blast is 5.0×10^4[Pa] at r = 0.020 [m] from the jet axis. It drops continuously as can be seen in the next two figures. In Figure 28, the first indication of a pressure plateau is in evidence which becomes very pronounced at t = 144.40 [μs] in Figure 29. By this time the pressure behind the blast had dropped to 1.0×10^4[Pa].

The flow exhibits analogous characteristics if one traverses it in the radial direction at a distance of 4.00×10^{-3}[m] from the propellant bag base surface. Again, as shown in Figure 30, after an initial pressure ramp at early times, clearly a blast wave develops which propagates rapidly outward. Later, for example at t = 102.63 [μs] in Figure 31, subatmospheric conditions prevail behind the blast followed by a pressure rise back to the vent hole conditions as one moves toward the jet axis. In these diagrams the pressure ramp is a consequence of the diffusion of the wave.

The next series of diagrams, Figures 33 through 35, show the velocity distribution along the jet axis. Again, after an initial transient, the maximum velocity stays at 1200 $[\frac{m}{s}]$.

In Figure 36 a comparison is shown between the calculated and the observed temporal distribution of the pressure at a location of 0.05 [m] radially from the tube axis at the base of the propellant bag (Figure 1 gage P_5). Stiefel's data[9] shows a pressure peak of 2.48×10^5[Pa] at 0.6 [ms] with a squared cone exit. For a straight-through hole, the peak pressure was observed at a later time, somewhere between 1.2 and 1.6 [ms]. On the other hand, the peak pressure did not seem to be influenced appreciably by the geometry of the vent hole. We see that the calculated pressure follows closely the observed behavior. The only difference is that after 100 [μs], the calculated pressure drops off more steeply than the measured value. The difference between the calculated and the experimental values at these late times may be due to the frequency response of the gage.

The temperature along the base of the propellant bag measured from the centerline of the bag reflects the passing of the blast wave and, later, the propellant gases. Starting at the stagnation point and moving radially, one notices the first local temperature maximum at around 5.0×10^{-3}[m] which remains in the same location from t = 16.78 [μs] to the termination of the computer run. This evidence points to the presence of a shock, made plausible by the arguments advanced in Chapter II, Section A-3, of this report.

The second local temperature maximum is observed at each time frame at the location of the blast wave where the temperature is near 1100[K]. The temperature data for several times is summarized below in Table II.

Table II. Temperature Along the Base Pad

Time [μs]	60.66	102.63	144.40
Location [m]	T[K]	T[K]	T[K]
0.001	629.58	617.18	604.47
0.005	736.10	721.52	706.61
0.010	739.47	724.86	709.89
0.015	720.96	706.75	692.16
0.020	696.59	682.88	668.80
0.025	674.28	656.51	643.00
0.030	1045.58	629.41	616.39
0.035	665.05	639.27	590.40
0.040	477.18	1070.07	755.94
0.045	301.57	814.12	1015.38
0.050		480.78	850.85
0.055		398.85	544.92
0.060		367.85	398.97
0.065		300.62	357.66
0.070			322.29
0.075			340.20
0.080			300.61
0.085			300.00

These temperatures should not be considered as absolute values but rather as indicative of the thermodynamic state at that particular time and place. As pointed out earlier, the temperature is a derived quantity, obtained from the equation-of-state. Depending on the value of the molecular weight of the product gases, the temperature can be made to vary by a factor of two. The controversial point is the question whether solids are precipitated as products of the reaction, and if so, in what quantities. A judgment of the accuracy of the temperature prediction has to await the resolution of this kinetics question.

It should be kept in mind that all of the foregoing results were obtained under greatly simplifying assumptions; the most restrictive of these was the fact that only one species, i.e., only one value of γ was used for both the reactants and the ambient. The γ used was that of the high enthalpy gas. Thus, the ambient, though at the correct temperature, is at a pressure of 5.22×10^4[Pa] which is lower than atmospheric, leading to an artificially enhanced wave propagation through the medium.

While overall determination of the flow dynamics is not adversely affected by the stipulation of laminar flow and negligible transport effects, local behavior can be greatly distorted by these assumptions. The inclusion of these effects would require the solution of the Navier-Stokes equations with kinetics and a turbulence model. At the present time the interaction between turbulence and chemical reactions is incompletely understood.

Turbulence models for compressible flows[12,13] have been developed and applied with some degree of success to practical problems. However these theories, as yet, do not take cognizance of the presence of particulate matter in the flow.

The overriding interest in primer flow calculations is the possibility of the determination of the heat transfer to the propellant bed. Known correlations relating Nusselt to the Reynolds and Prandtl numbers of course require values of the transport coefficients which were not considered in this study[14,15]. However, from a study of the flow regime, one can make reasonable estimates of these and thus of the heat transfer. Ultimately, of course, the full three-dimensional, two-phase, unsteady, viscid, reactive flow equations will have to be solved for a complete resolution of the problem.

---

[12] Fernholz, H. H., "External Flows" in Turbulence, P. Bradshaw, Ed., Springer Verlag, Berlin, pp. 45-98, 1976.

[13] Coles, D. E., Hirst, E. A. (Eds.), Proceedings, Computation of Turbulent Boundary Layers - 1968 AFOSR-IFP Stanford Conference, Thermosciences Division, Stanford University, 1969.

[14] Rohsenow, W.M., Choi, H. Y., Heat, Mass and Momentum Transfer, Prentice-Hall, Inc., Englewood Cliffs, NJ, 1961.

[15] Afgan, N. H., Beer, J. M., Ed., Heat Transfer in Flames, John Wiley and Sons, New York, 1974.

IV. CONCLUSIONS

A theoretical program has been conducted to investigate the flow dynamics of an M-82 primer from the time that the primer propellant is ignited up to 144 [μs] after the gases have exited the vent hole and enveloped an inert propellant charge in the chamber of the gun. The results of this study indicate:

a. The gross features of the primer flow dynamics can be modeled adequately with off-the-shelf computer codes;

b. These results permit an overall assessment of primer functioning;

c. Comparison with experimental findings is only possible for some of the parameters of the problem;

d. Using available codes, parametric studies can be conducted which should point to modes of product improvement.

ACKNOWLEDGMENT

The author would like to thank Dr. A. K. R. Celmins, Mr. Monte Coleman and Dr. K. J. White for useful discussions in the course of the preparation of this report.

REFERENCES

1. Celmins, A.K.R., "RECRIF Users' Manual", BRL MR 2693, October 1976.

2. Farr, J.L. and Traci, R.M., "A Users' Manual for SAMS", BRL Contract Report 162, June 1974.

3. Rudinger, G., "Flow of Solid Particles in Gases", AGARDograph No. 222, AGARD, Neuilly Sur Seine, France, 1976.

4. Rudinger, G., "Some Effects of Finite Particle Volume on the Dynamics of Gas Particle Mixtures", AIAA Journal 3, 1217-1222, (1965).

5. Rudinger, G., "Relaxation in Gas-Particle Flow" in Nonequilibrium Flows, Part I, P.P. Wegener, Ed. Marcel Dekker, NY, 1969.

6. Federoff, B.T. and Sheffield, O.E., "Encyclopedia of Explosives and Related Items", Volume 2. Picatinny Arsenal, Dover, NJ, 1962.

7. Freedman, E., Private Communication.

8. Kalghatgi, G.T., Hunt, B.L., "The Occurence of Stagnation Bubbles in Supersonic Jet Impingment Flows", Aeronautical Quarterly, 27, 169-185, 1976.

9. Stiefel, L., "Experimental Characterization of the Output of Artillery Primers" (to be published).

10. White, K.J., Hartman, R.A., May, I.W., Kelso, J.R., "Experimental Investigation of Ignition Train System for Bagged Charges", 14th JANNAF Combustion Meeting, (in press), 1977.

11. White, J.J., Price, C.F., Holmes, H.E., May, I.W., "Black Powder and Clean Burning Ignitor Ignition Train Studies", 13th JANNAF Combustion Meeting, Vol. I. pp. 405-423, CPIA, Laurel, MD, 1976.

12. Fernholz, H. H., "External Flows" in Turbulence, P. Bradshaw, Ed., Springer Verlag, Berlin, pp. 45-98, 1976.

13. Coles, D. E., Hirst, E. A. (Eds.), Proceedings, Computation of Turbulent Boundary Layers - 1968 AFORS-IFP Stanford Conference, Thermosciences Division, Stanford University, 1969.

14. Rohsenow, W. M., Choi, H. Y., Heat, Mass and Momentum Transfer, Prentice-Hall, Inc., Englewood Cliffs, NJ, 1961.

15. Afgan, N. H., Beer, J. M., Ed., Heat Transfer in Flames, John Wiley and Sons, New York, 1974.

APPENDIX

ILLUSTRATIONS

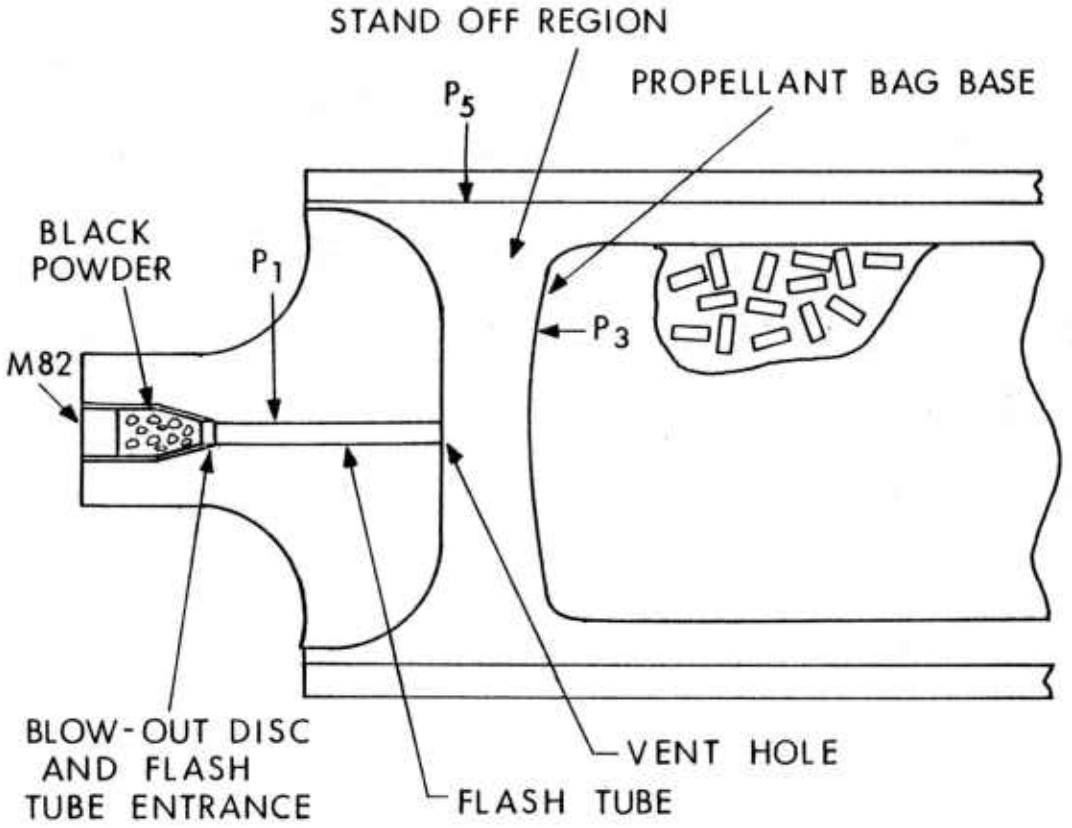

Figure 1. Schematic of the initiator spindle assembly for the 155mm howitzer. P_1 and P_5 indicate the location of the pressure transducers (Reference 9).

a

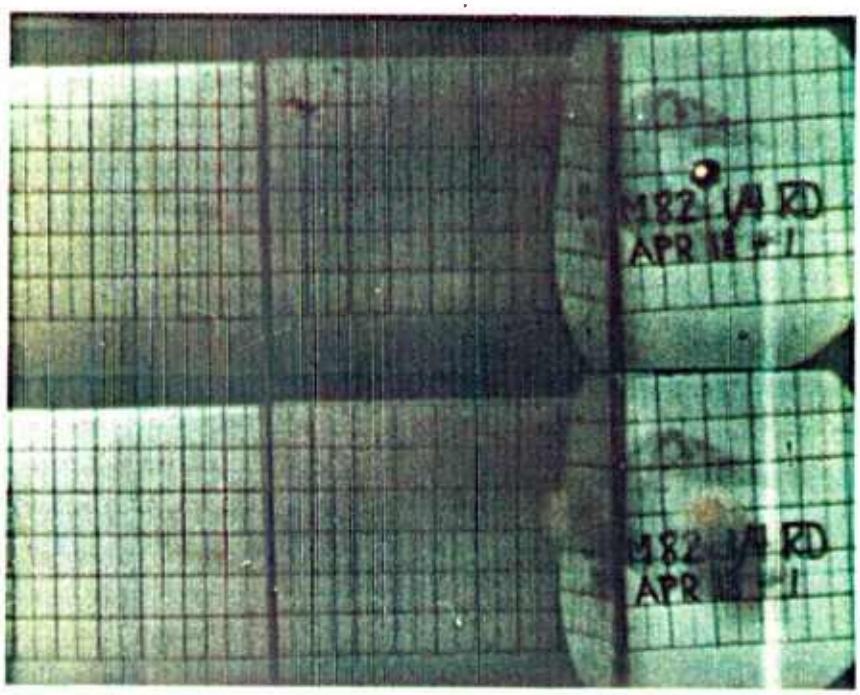

b

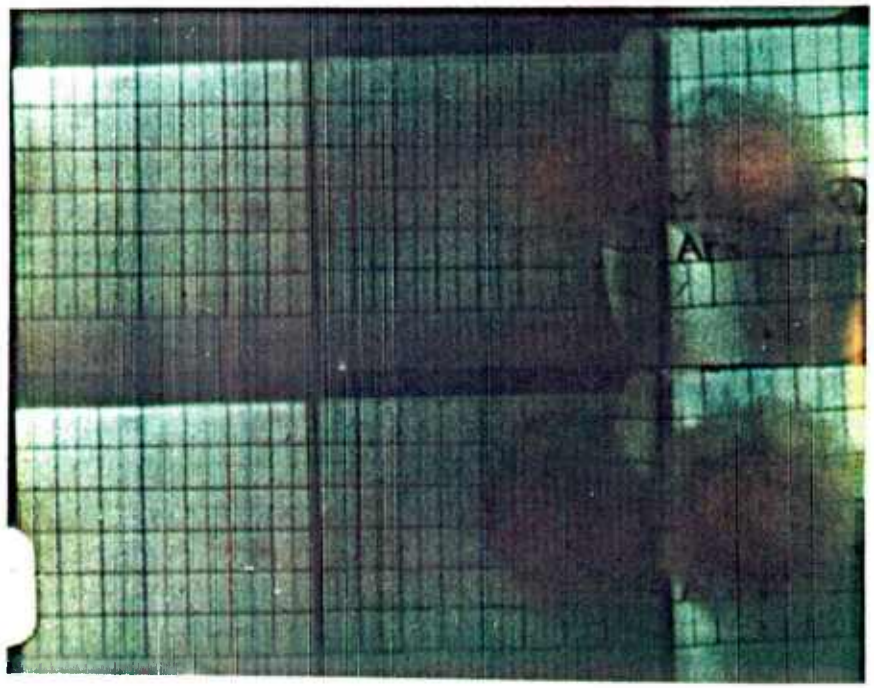

Figure 2. The development of the flow at the vent hole. (a) t = 0, 52.9 [μs]; (b) t = 106, 159 [μs]; (c) t = 212, 265 [μs]; (d) t = 317, 370 [μs]. Right-hand side of photo is viewed from 90°. Each small division represents 1.0×10^{-2} [m]. Photographs courtesy of Dr. K. J. White, Propulsion Division, BRL.

c

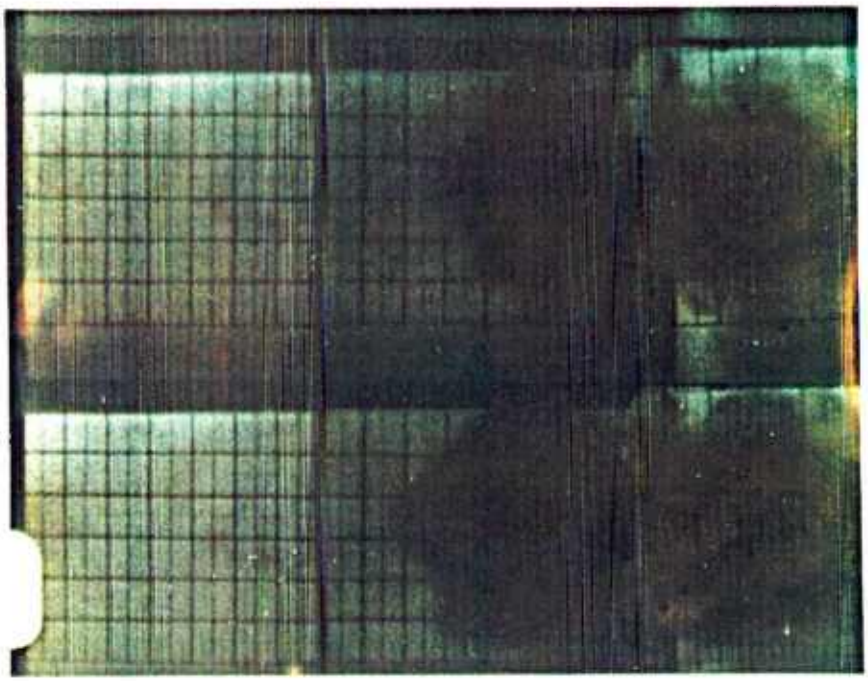

d

Figure 2 (Cont'd)

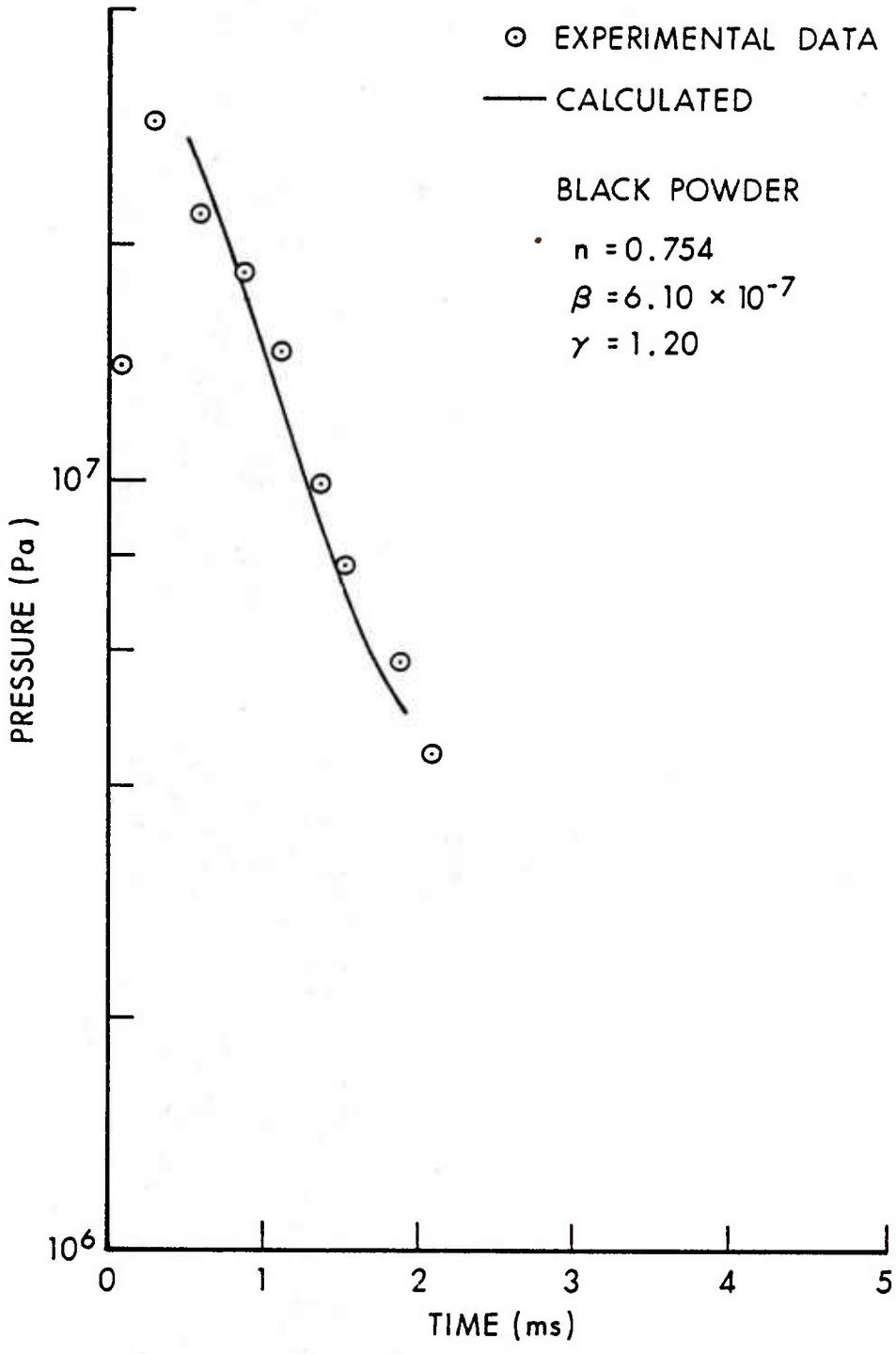

Figure 3. Comparison of calculated and experimentally observed pressure time history for black powder at a station 0.084 [m] from the primer combustion chamber. Experimental data courtesy of Dr. K. J. White, Propulsion Division, BRL.

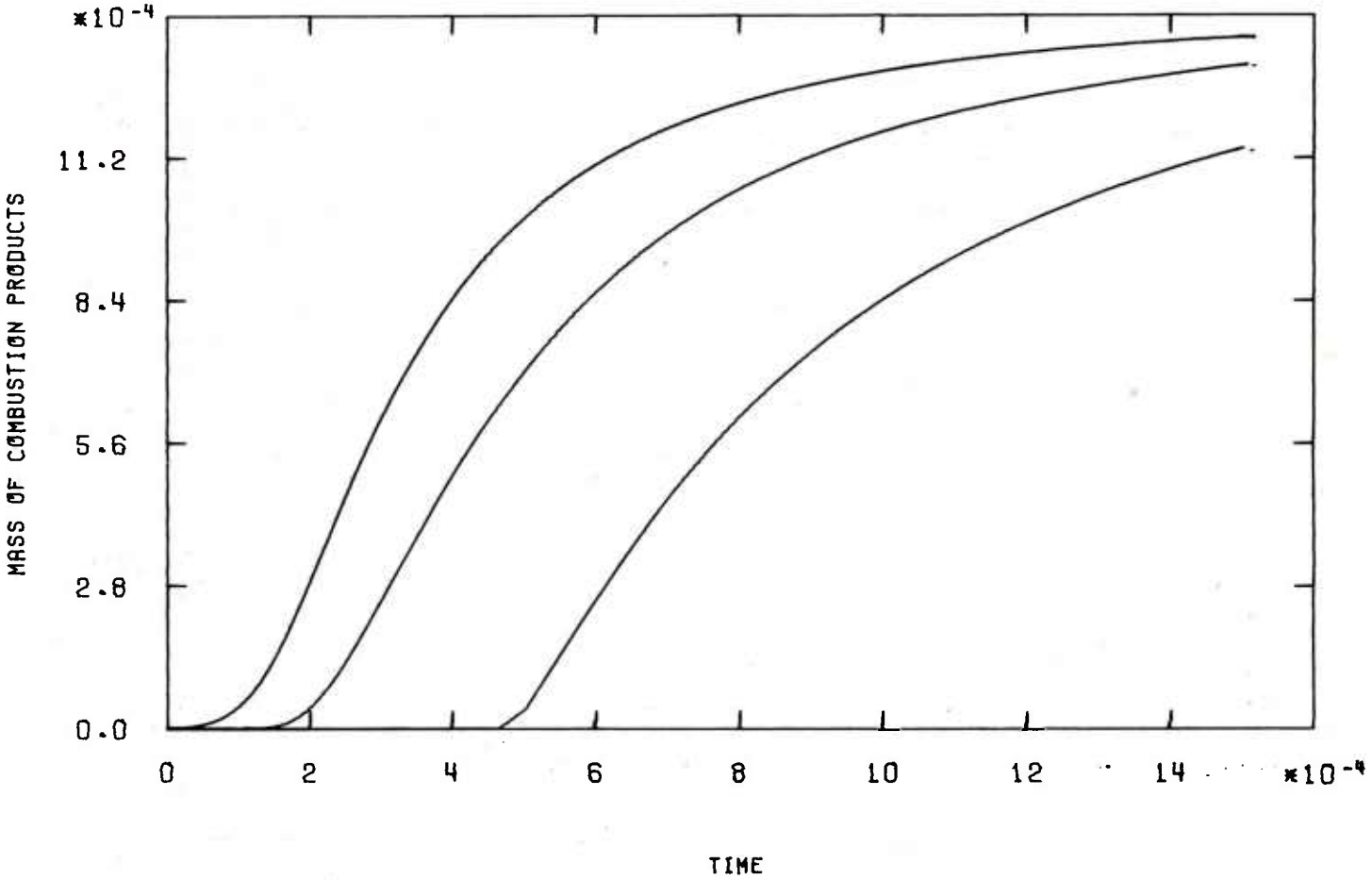

Figure 4. Mass of combustion products in [kg] as a function of time in [s] in the flash tube.

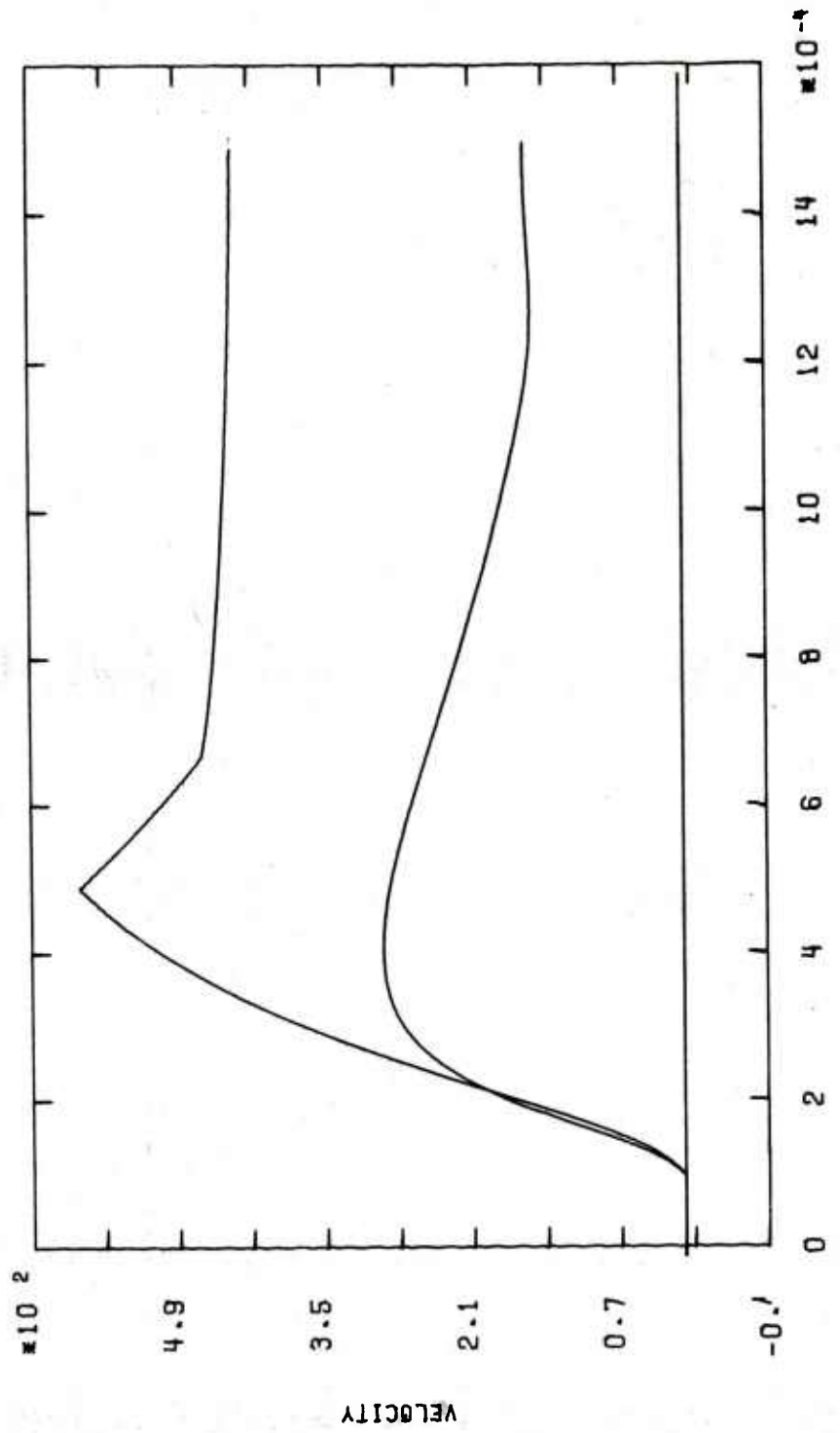

Figure 5. Gas velocity in $[\frac{m}{s}]$ as a function of time in [s].

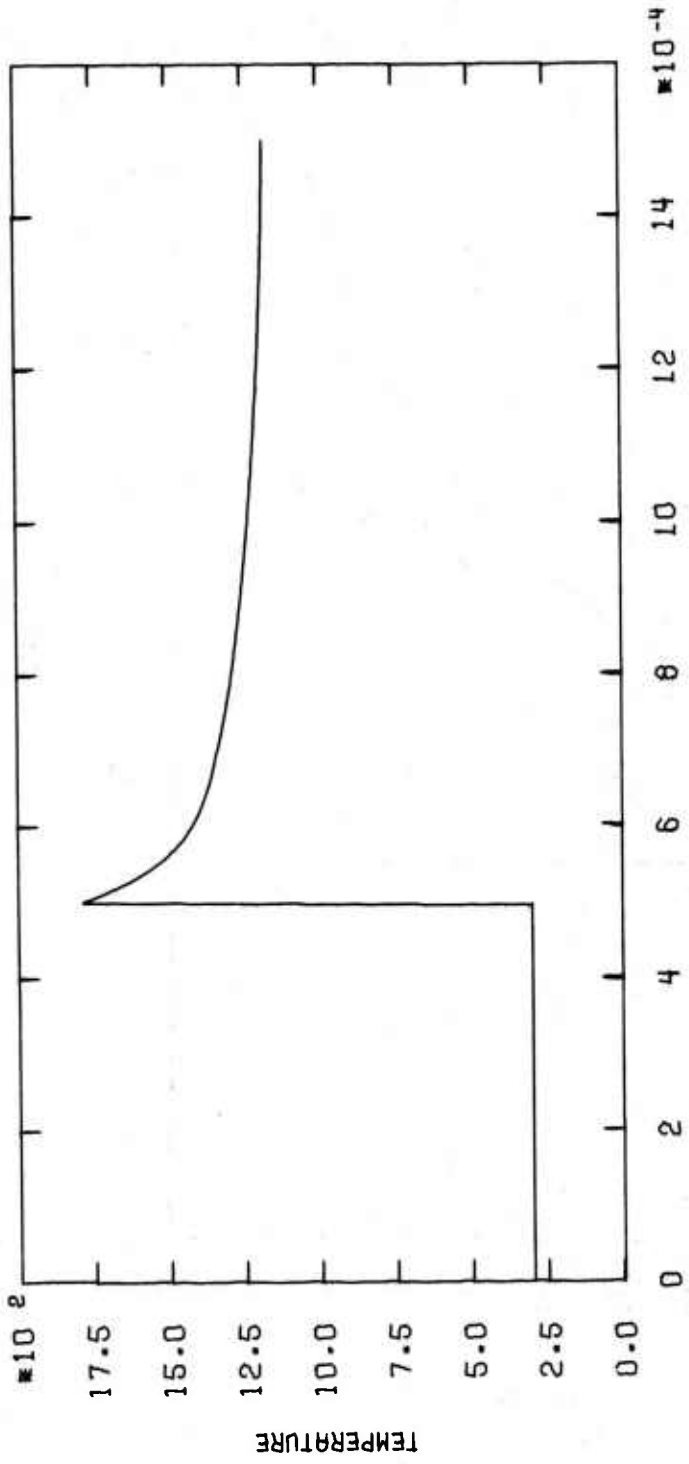

Figure 6. Vent hole temperature in degrees [K] as a function of time expressed in [s].

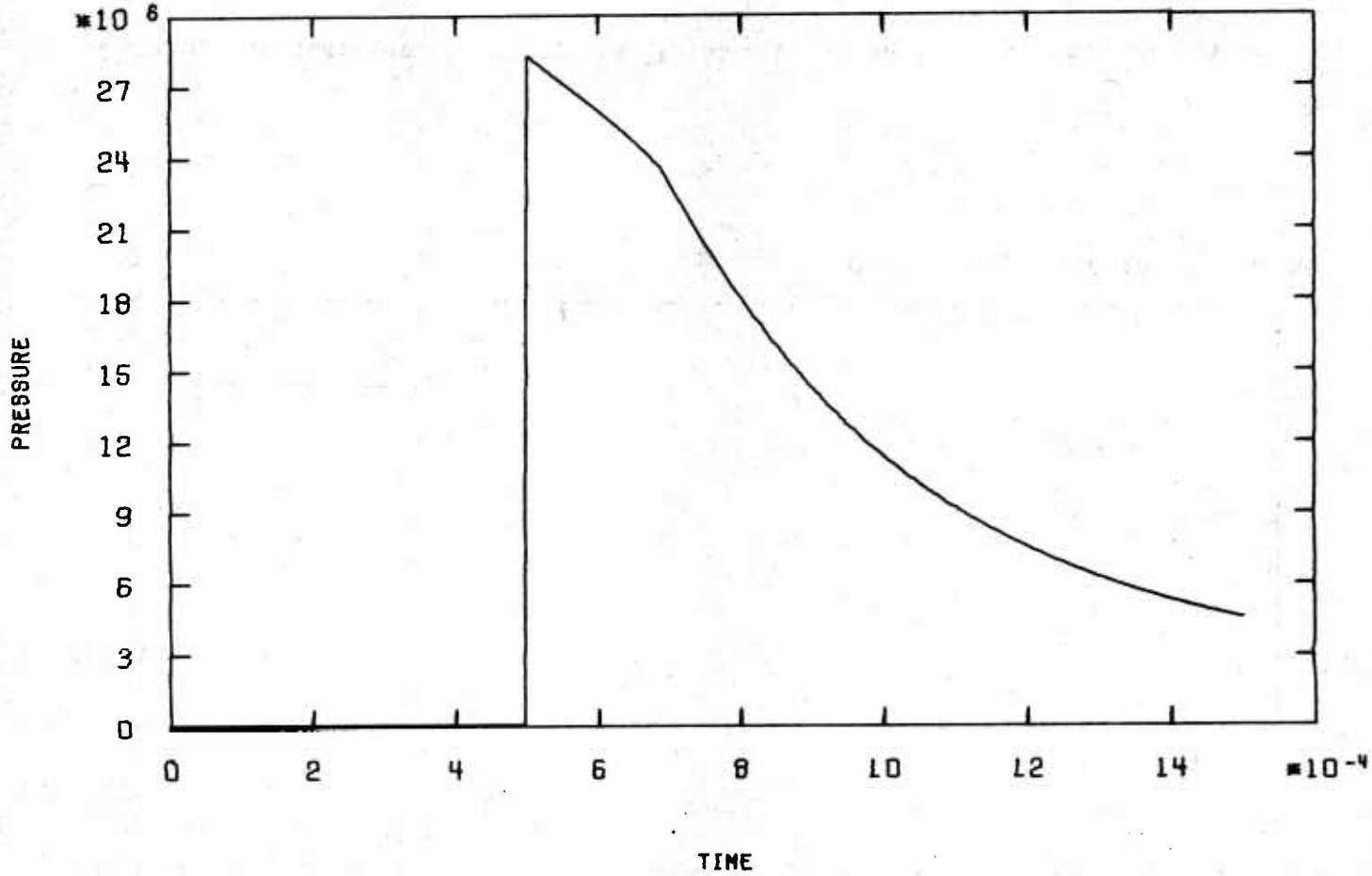

Figure 7. Vent hole pressure in units of [Pa] as a function of time in [s].

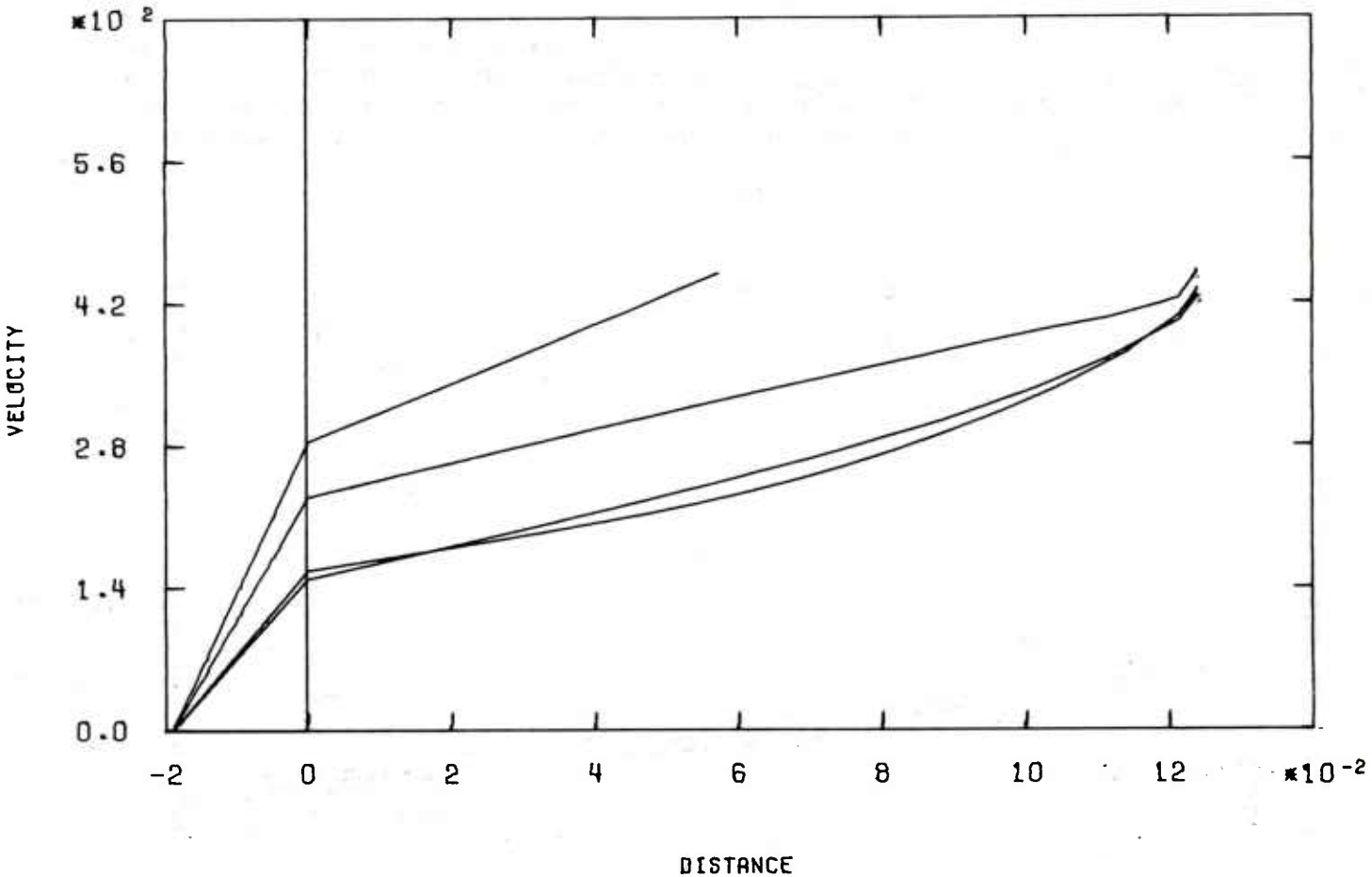

Figure 8. The gas velocity in the primer combustion chamber and the flash tube. The vertical line denotes the entrance to the flash tube. Units are $[\frac{m}{s}]$ and [m] respectively. From top to bottom the curves refer to t = 3.733×10^{-4}, 7.466×10^{-4}, 1.120×10^{-3} and 1.493×10^{-3}[s] respectively.

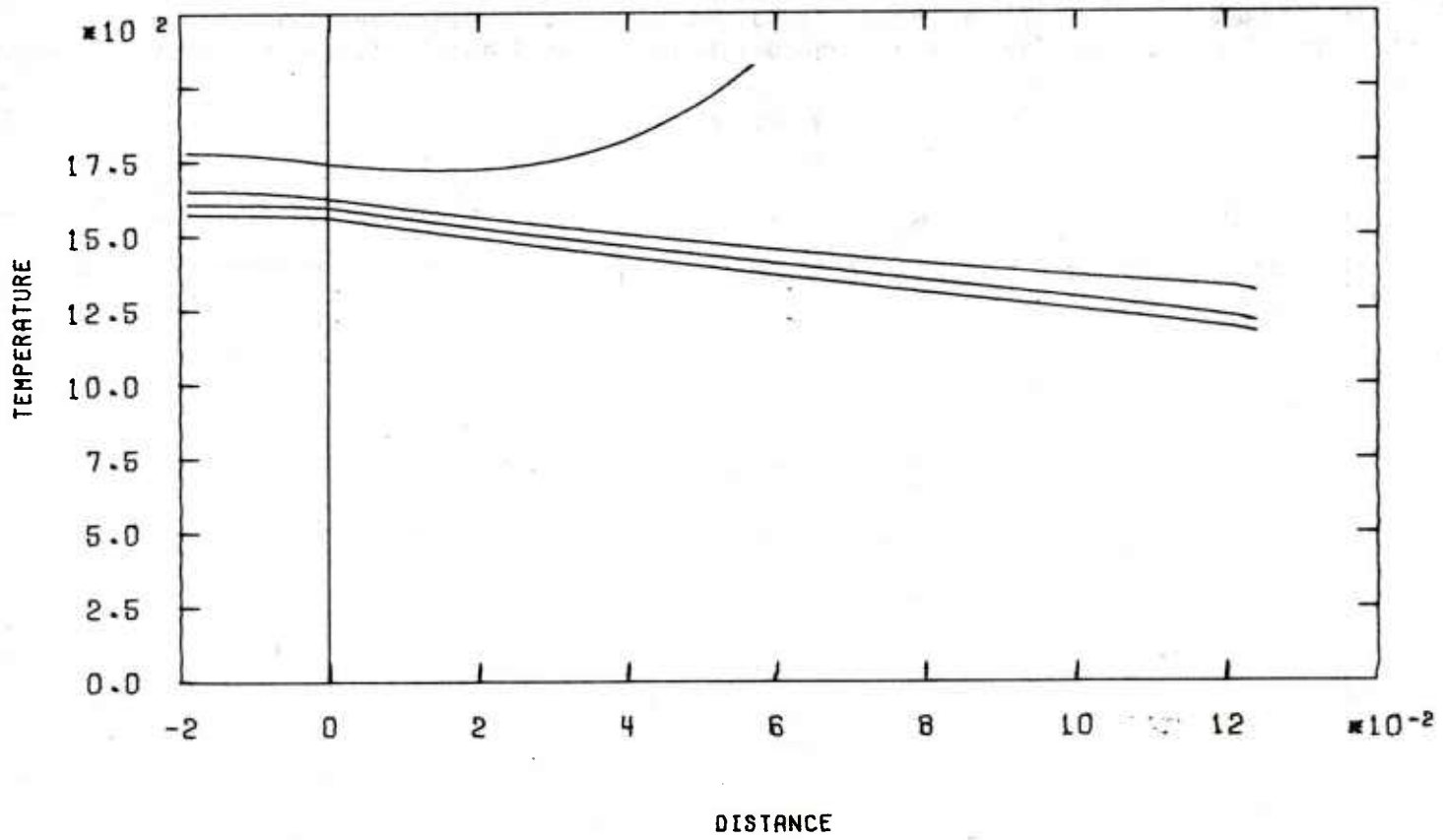

Figure 9. Temperature in the chamber and the flash tube as a function of location. The vertical line denotes the entrance to the flash tube. Units are [K] and [m] respectively. From top to bottom the curves refer to $t = 3.733 \times 10^{-4}$, 7.466×10^{-4}, 1.120×10^{-3} and 1.493×10^{-3}[s] respectively.

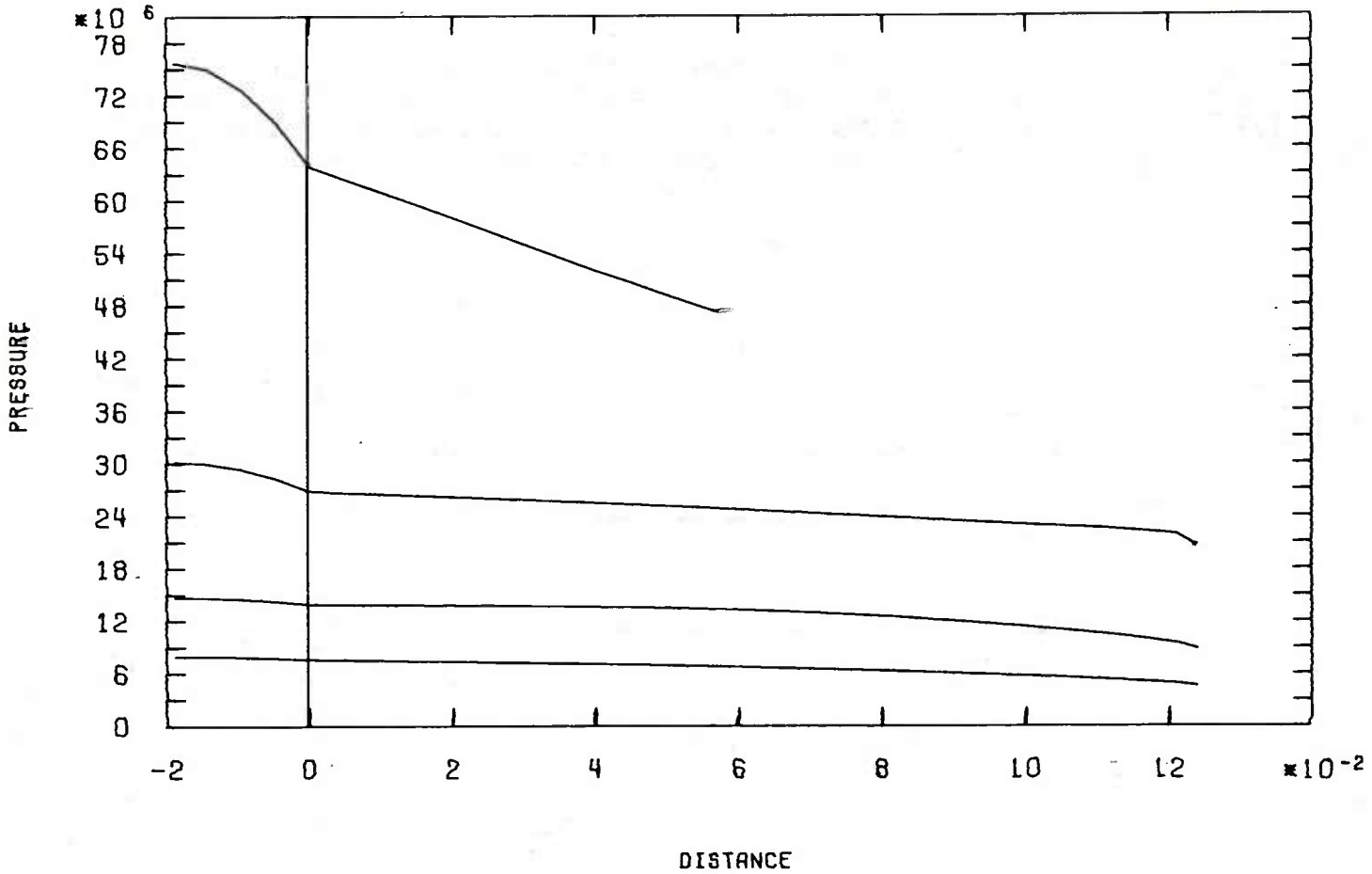

Figure 10. Pressure in the chamber and the flash tube as a function of location. The vertical line denotes the entrance to the flash tube. Units are [Pa] and [m] respectively. From top to bottom the curves refer to t = 3.733×10^{-4}, 7.466×10^{-4}, 1.120×10^{-3} and 1.493×10^{-3}[s] respectively.

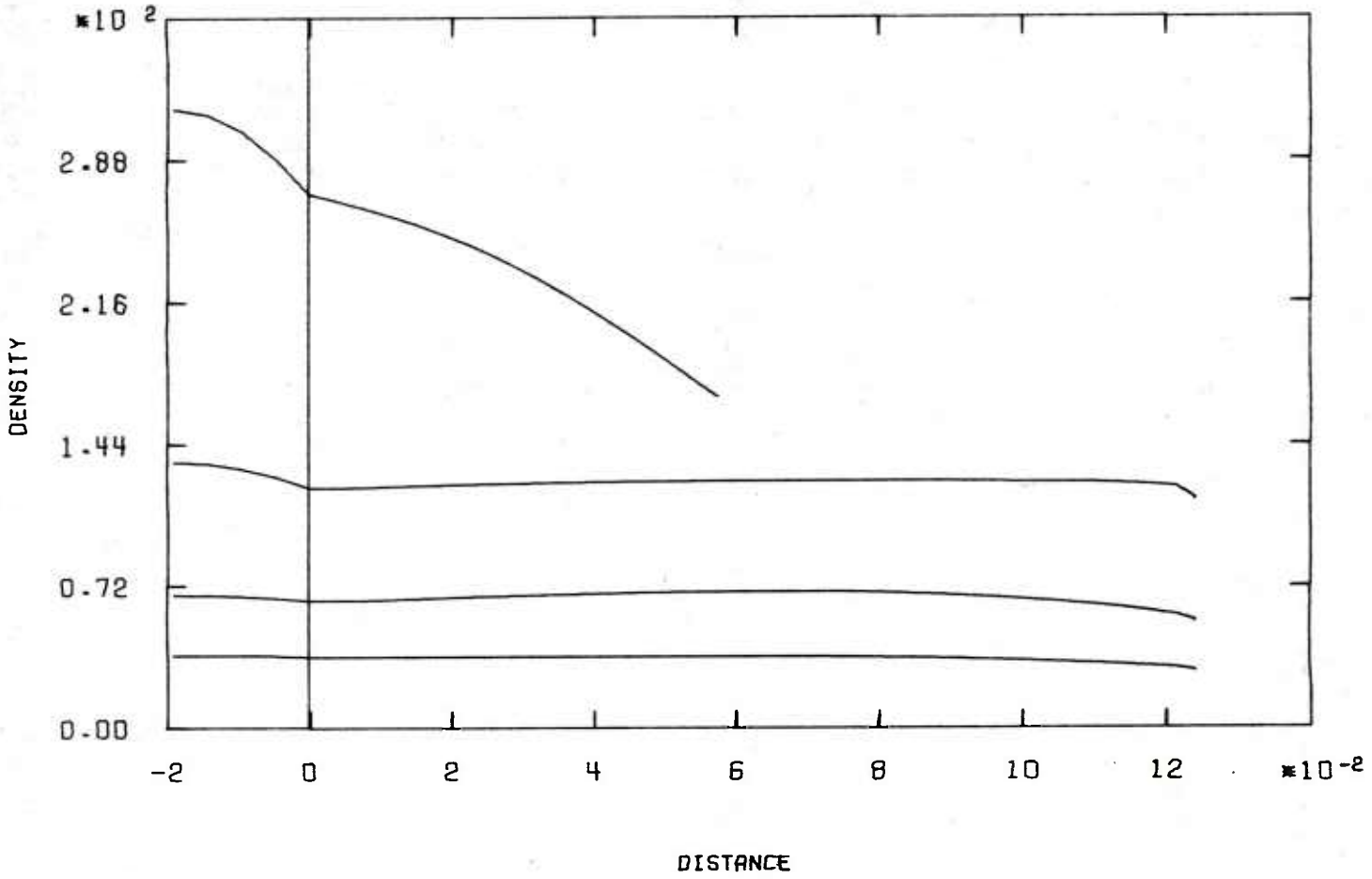

Figure 11. Density in the primer combustion chamber and the flash tube as a function of location. The vertical line denotes the entrance to the flash tube. Units are [kg/m^3] and [m] respectively. From top to bottom the curves refer to 3.733×10^{-4}, 7.466×10^{-4}, 1.120×10^{-3} and 1.493×10^{-3}[s] respectively.

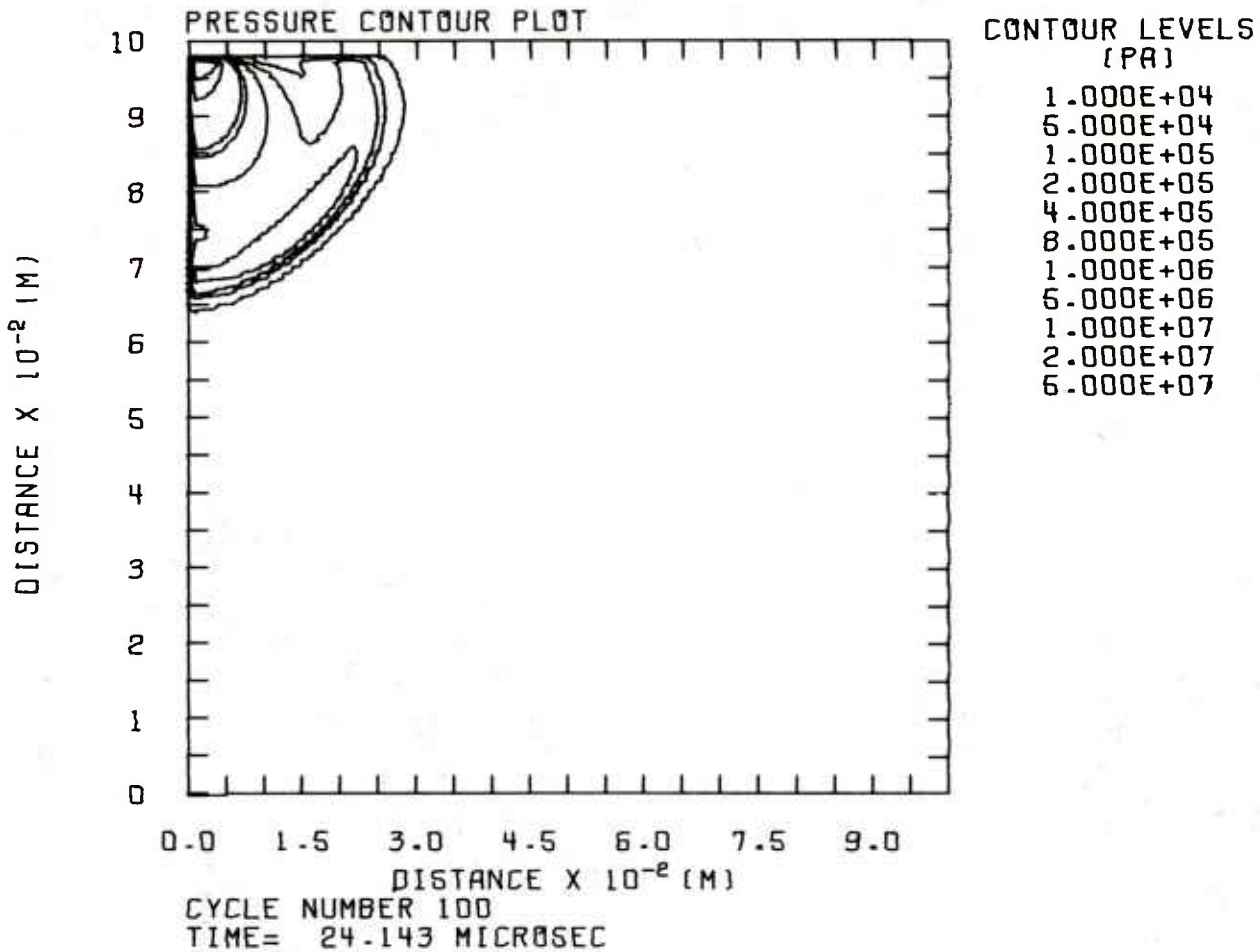

Figure 12. Free jet pressure contour plot at t = 23.14 [μs]. Vent hole located in the upper left hand corner of the plot is facing downward.

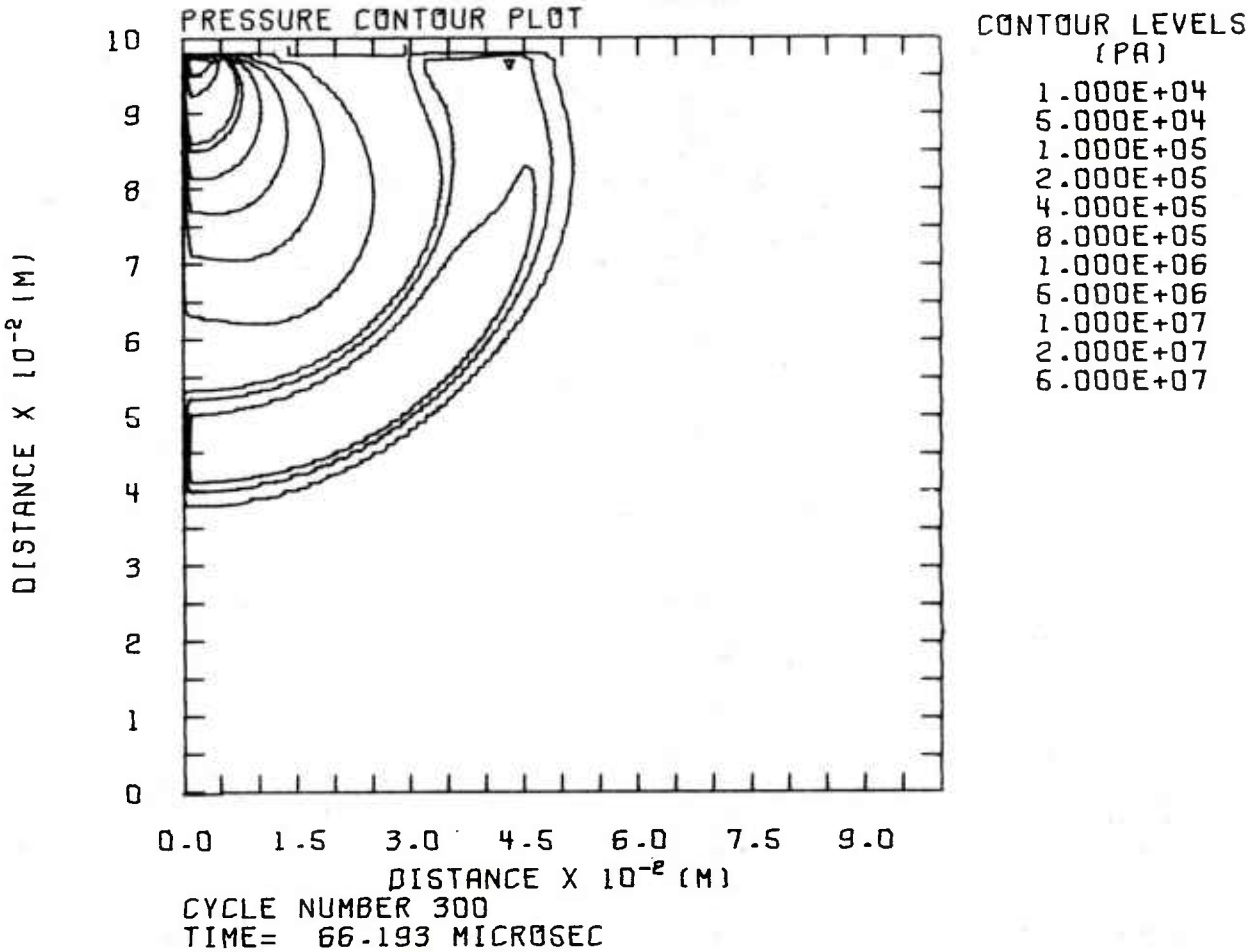

Figure 13. Free jet pressure contour plot at t = 66.19 [μs].

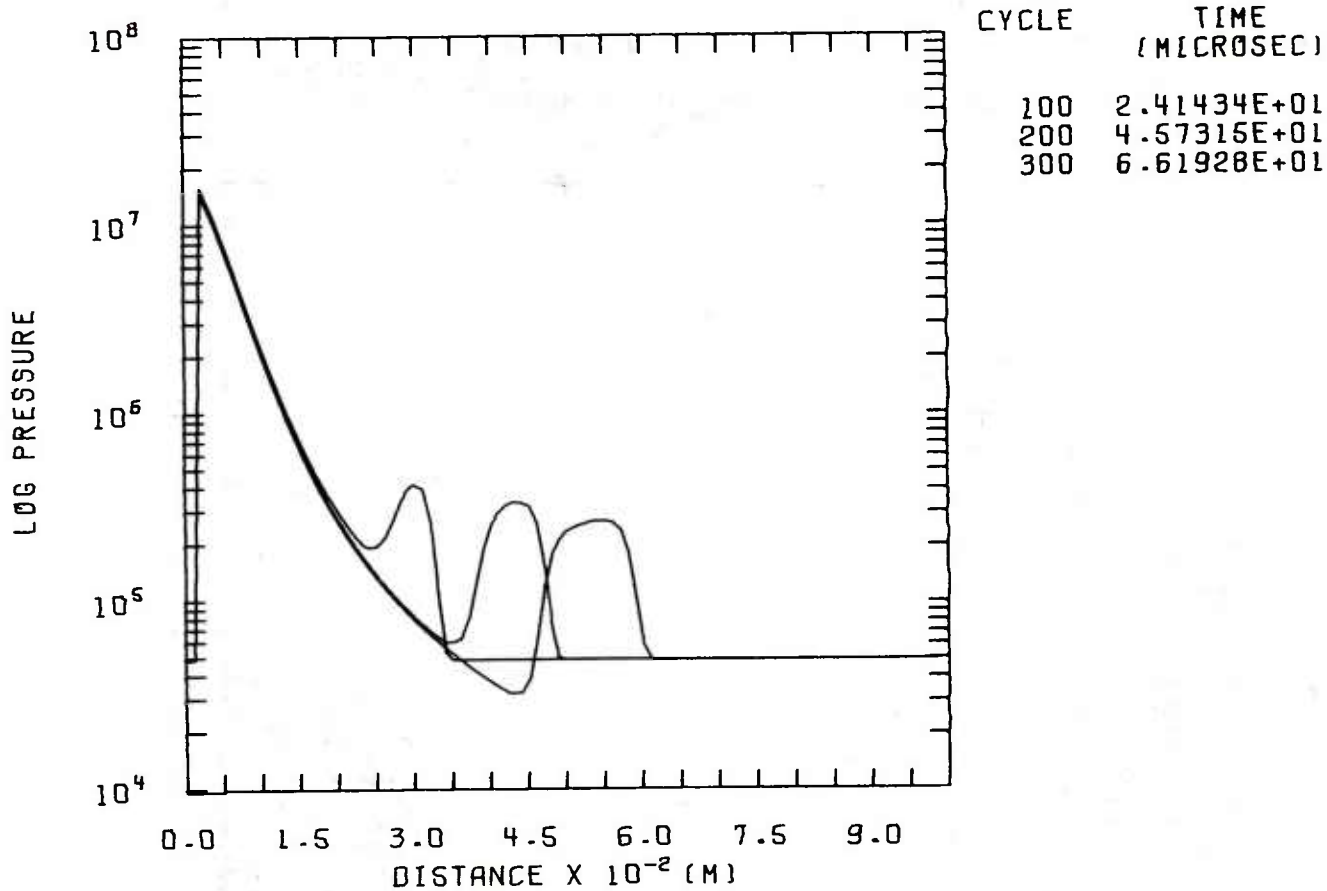

Figure 14. Pressure vs distance along the jet axis.

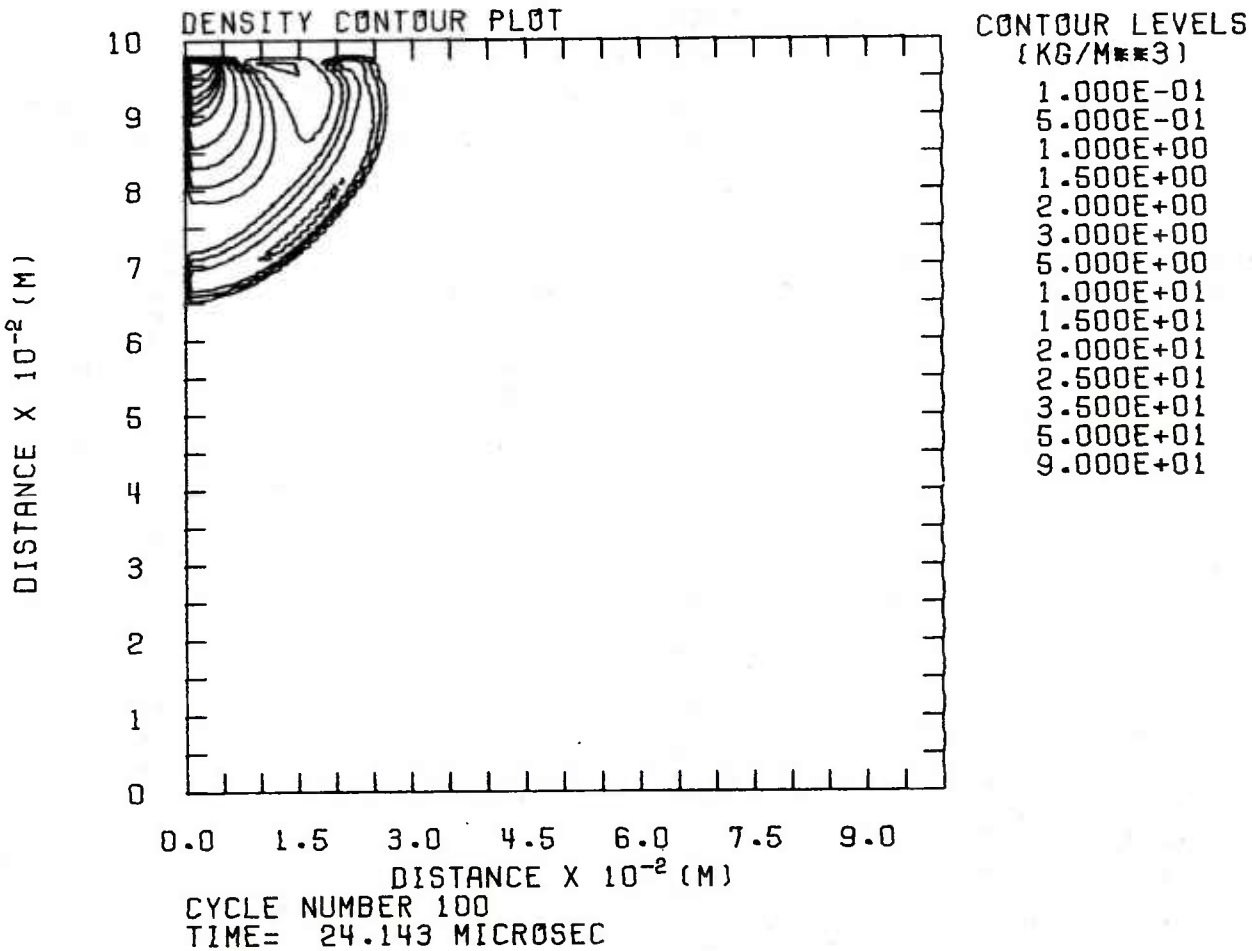

Figure 15. Free jet density contour plot at t = 24.14 [μs].

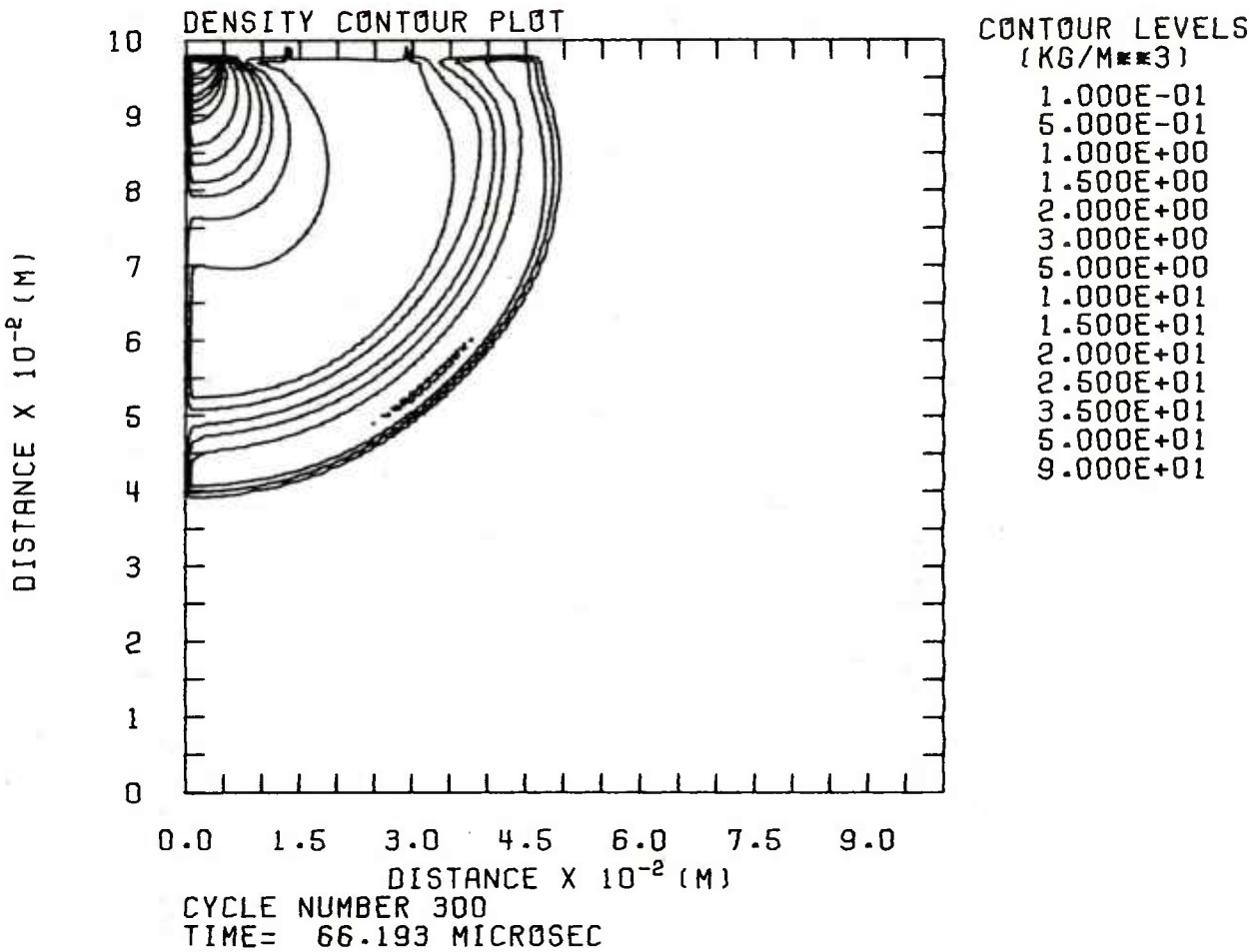

Figure 16. Free jet density contour plot at t = 66.19 [μs].

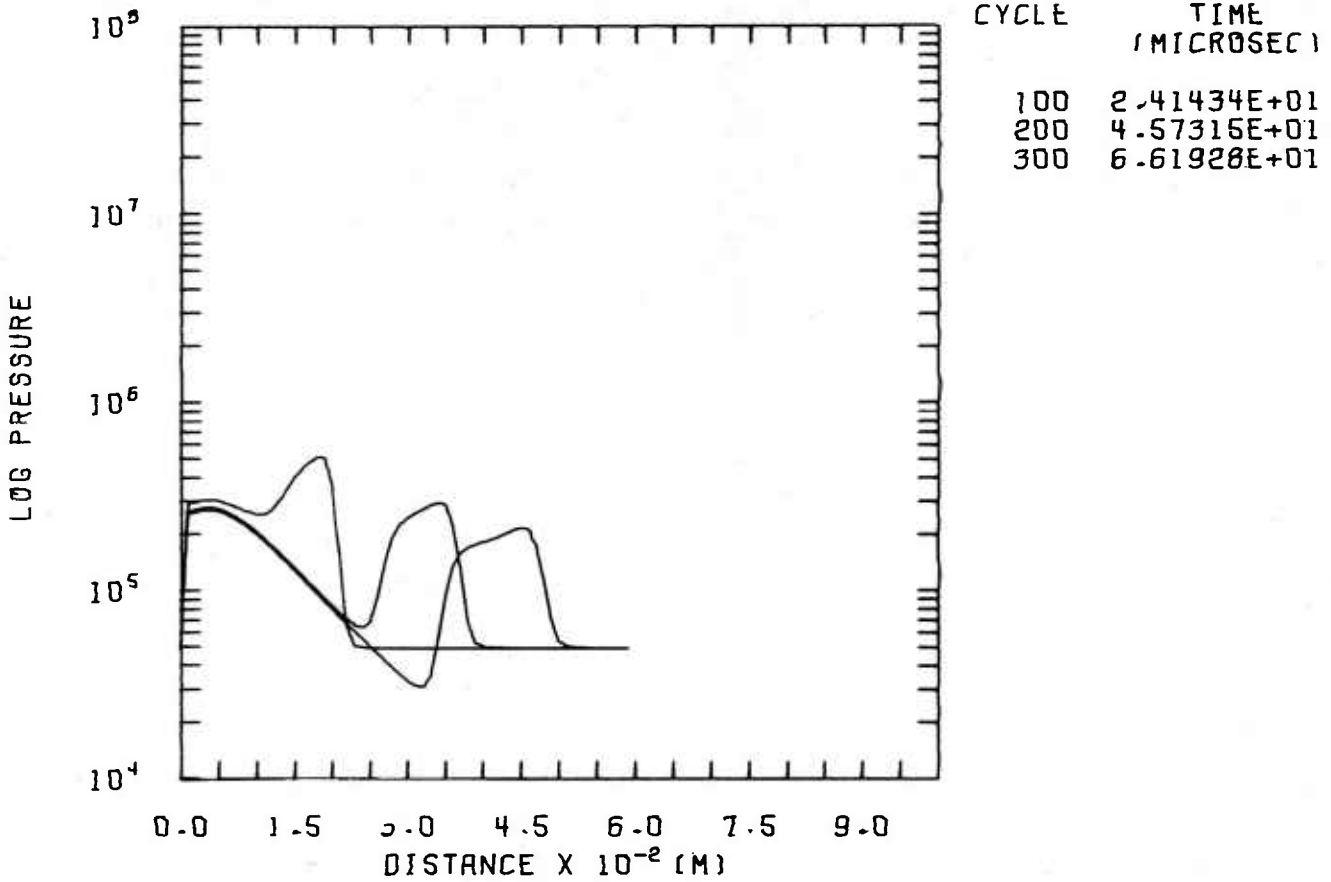

Figure 17. Pressure radially across the free jet at 1.9 x 10^{-2}[m] from the plane of the vent hole.

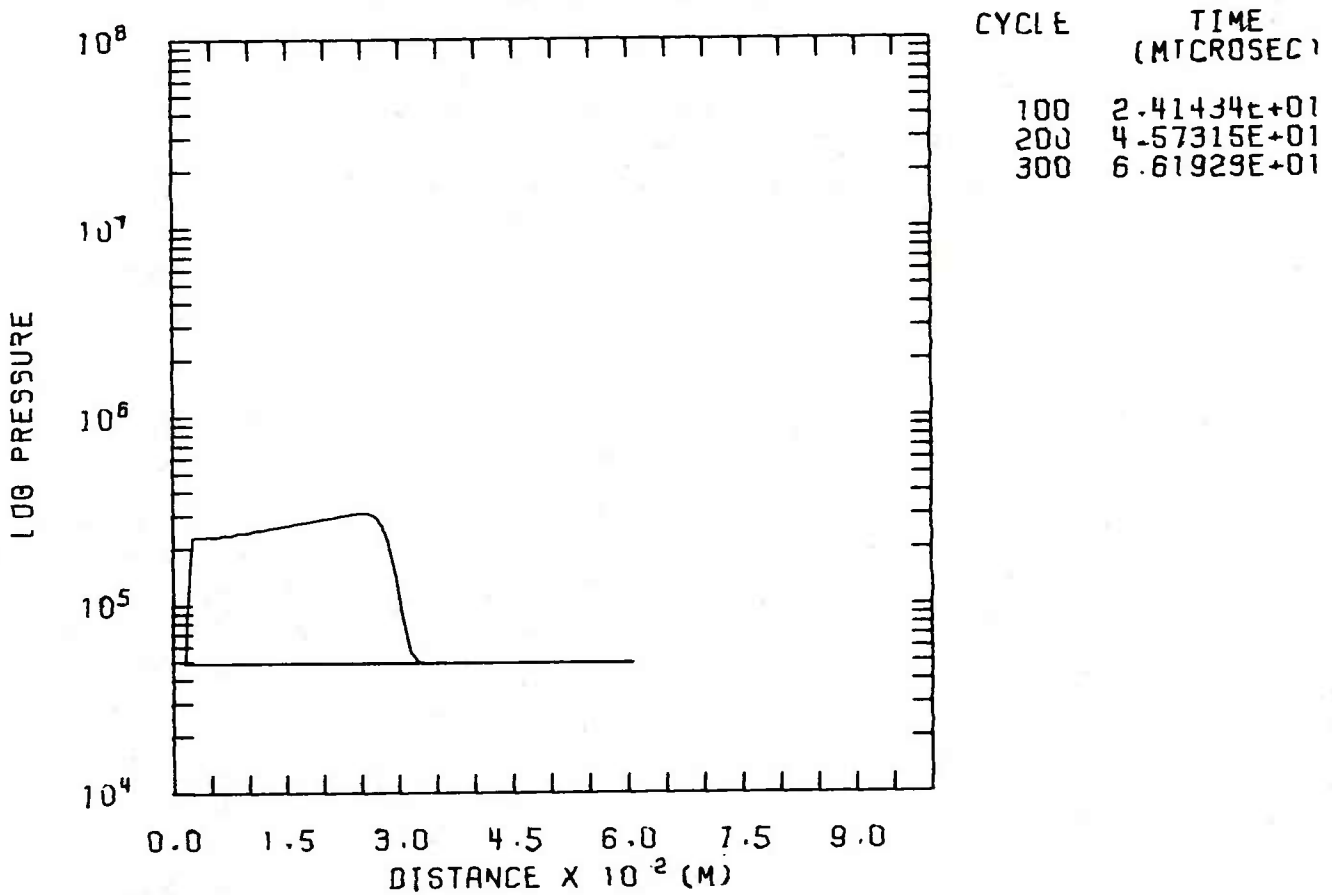

Figure 18. Pressure radially across the free jet at 4.9×10^{-2}[m] from the plane of the vent hole.

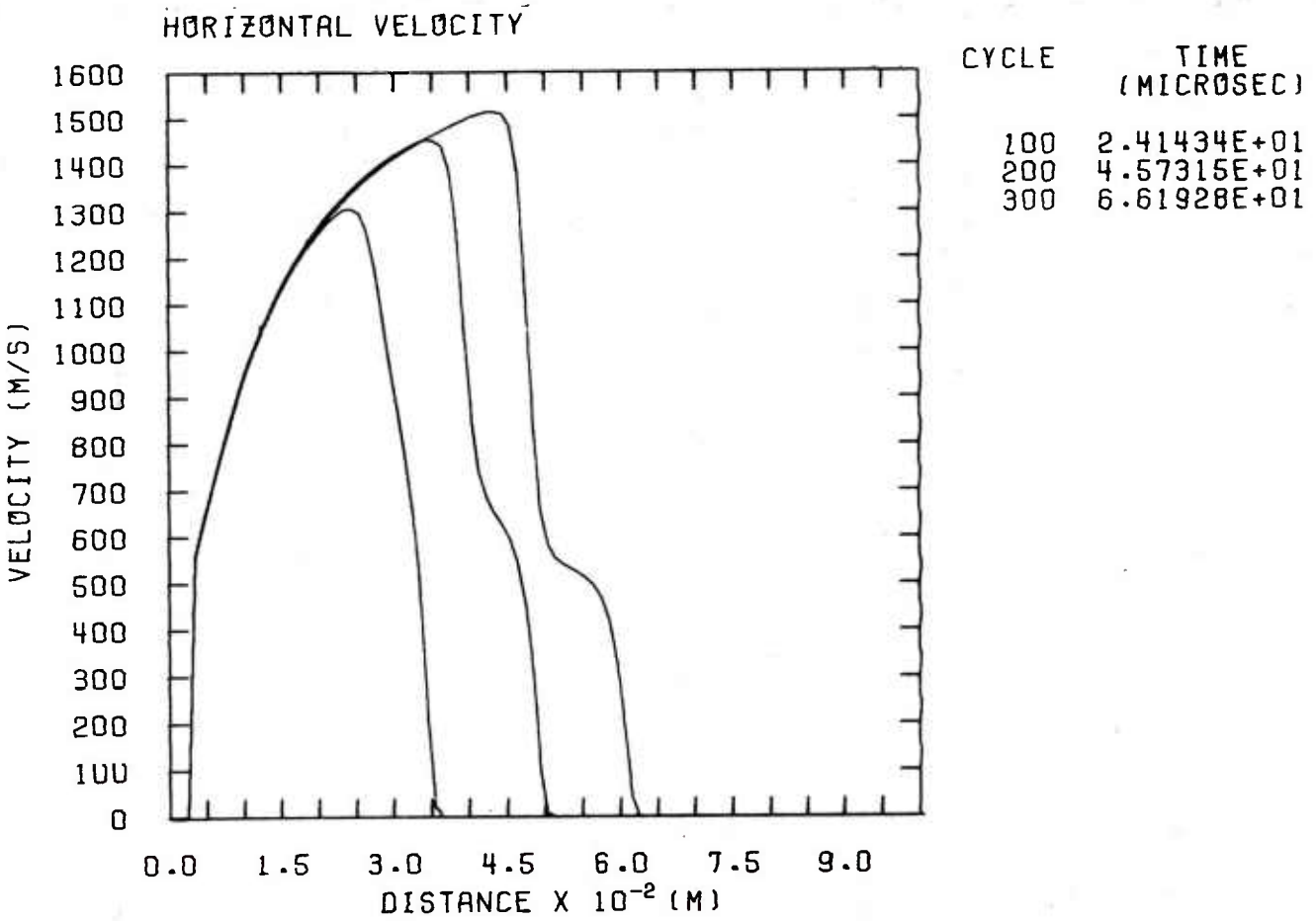

Figure 19. Velocity along the free jet axis at t = 24.14, 45.73 and 66.19 [μs] respectively.

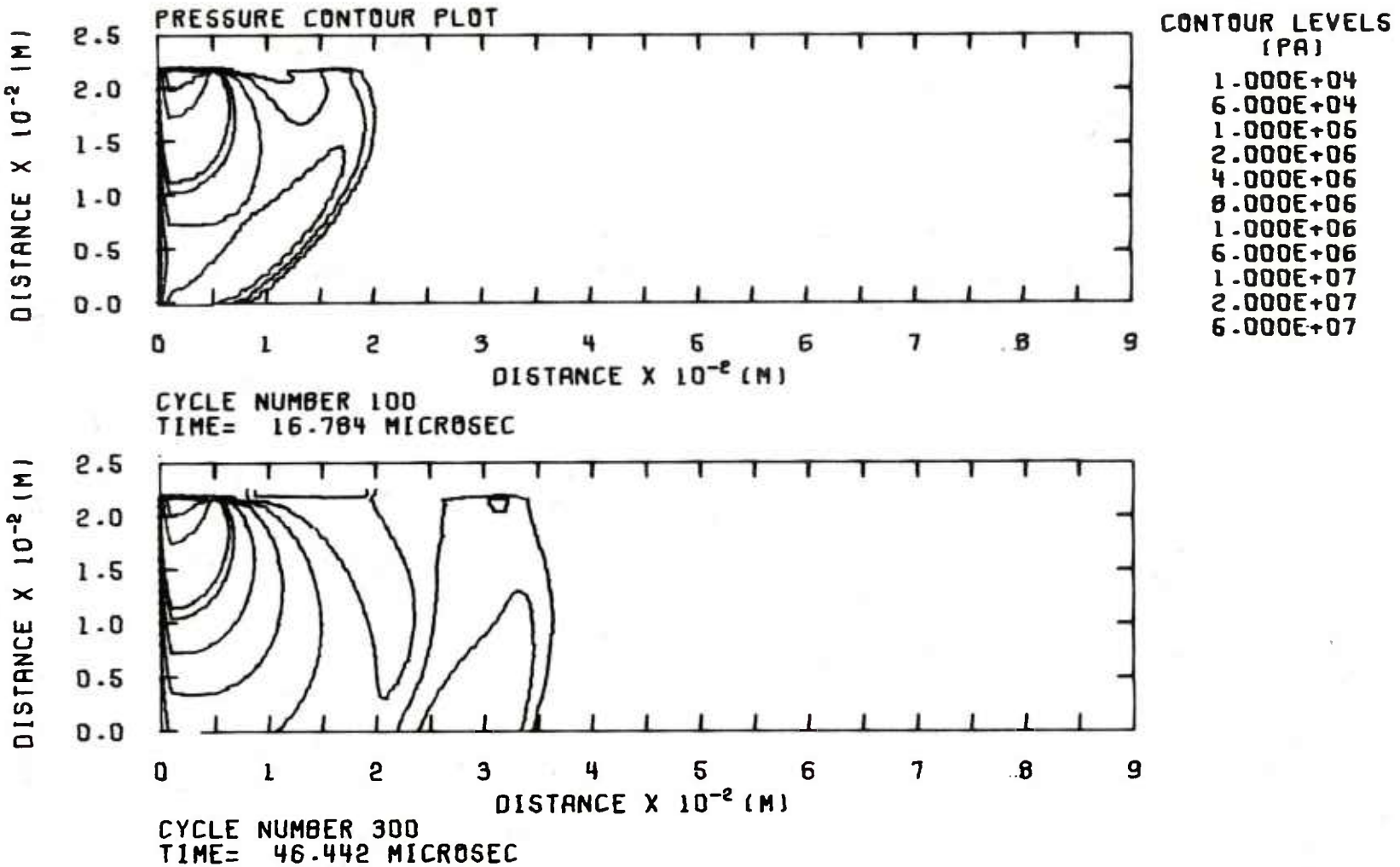

Figure 20. Pressure contour plots of the primer jet in the stand-off region at t = 16.78 and 46.44 [μs]. The vent hole is located in the upper left hand corner. The lower boundary represents the propellant bag and the left hand boundary is the axis of the jet.

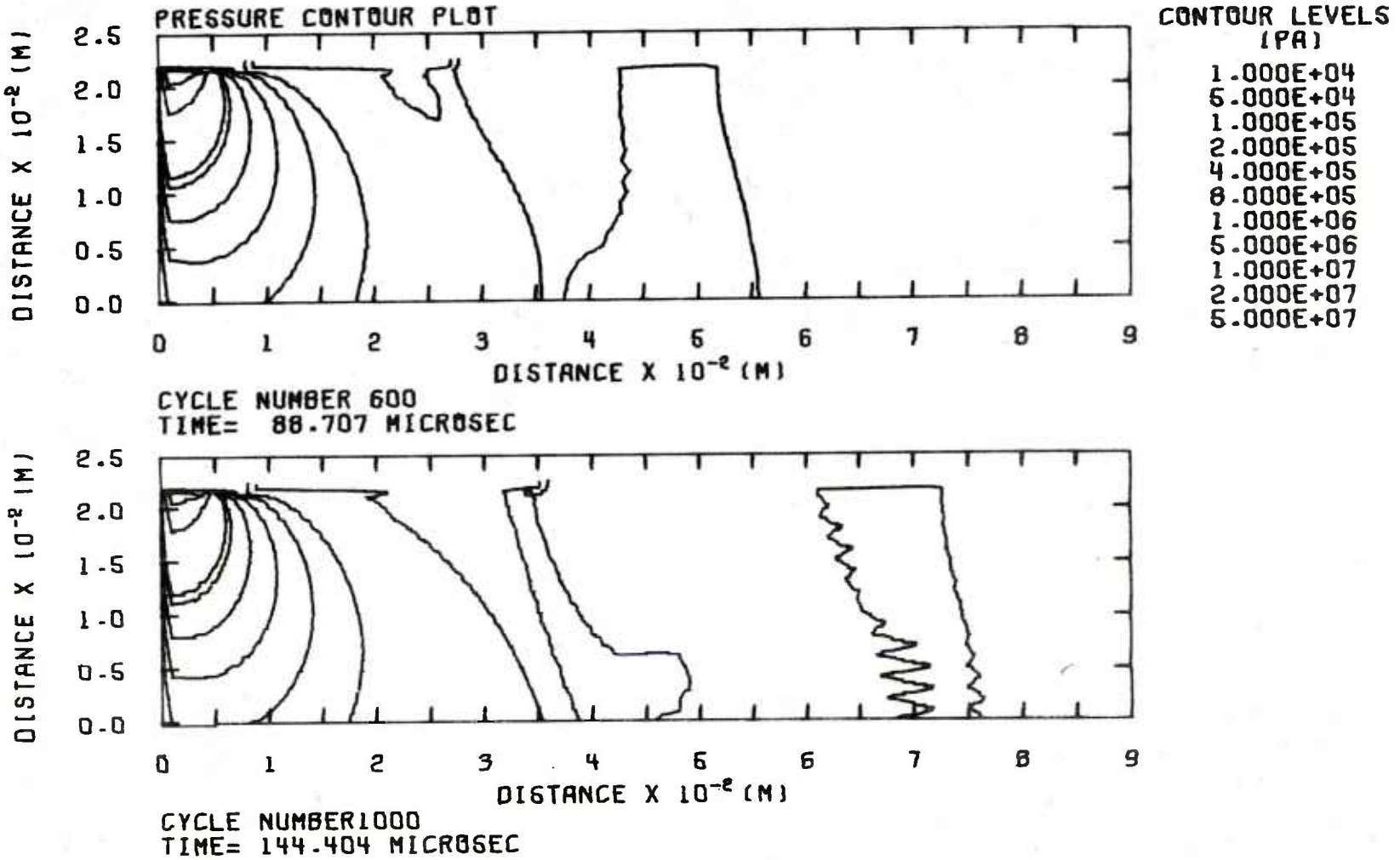

Figure 21. Pressure contour plots of the primer jet in the stand-off region at t = 88.70 and 144.40 [μs].

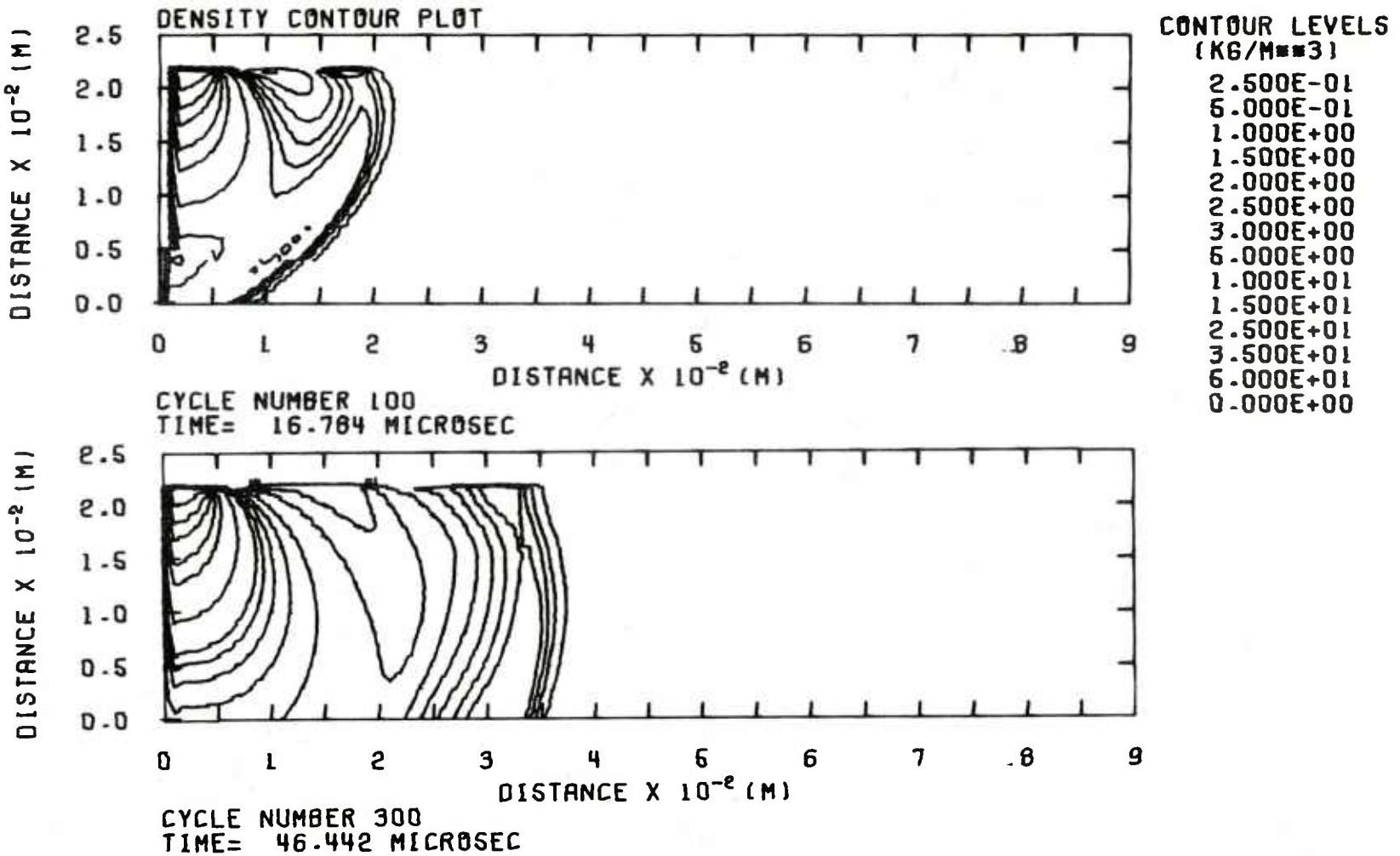

Figure 22. Density contour plots of the primer jet in the stand-off region at t = 16.78 and 46.44 [μs].

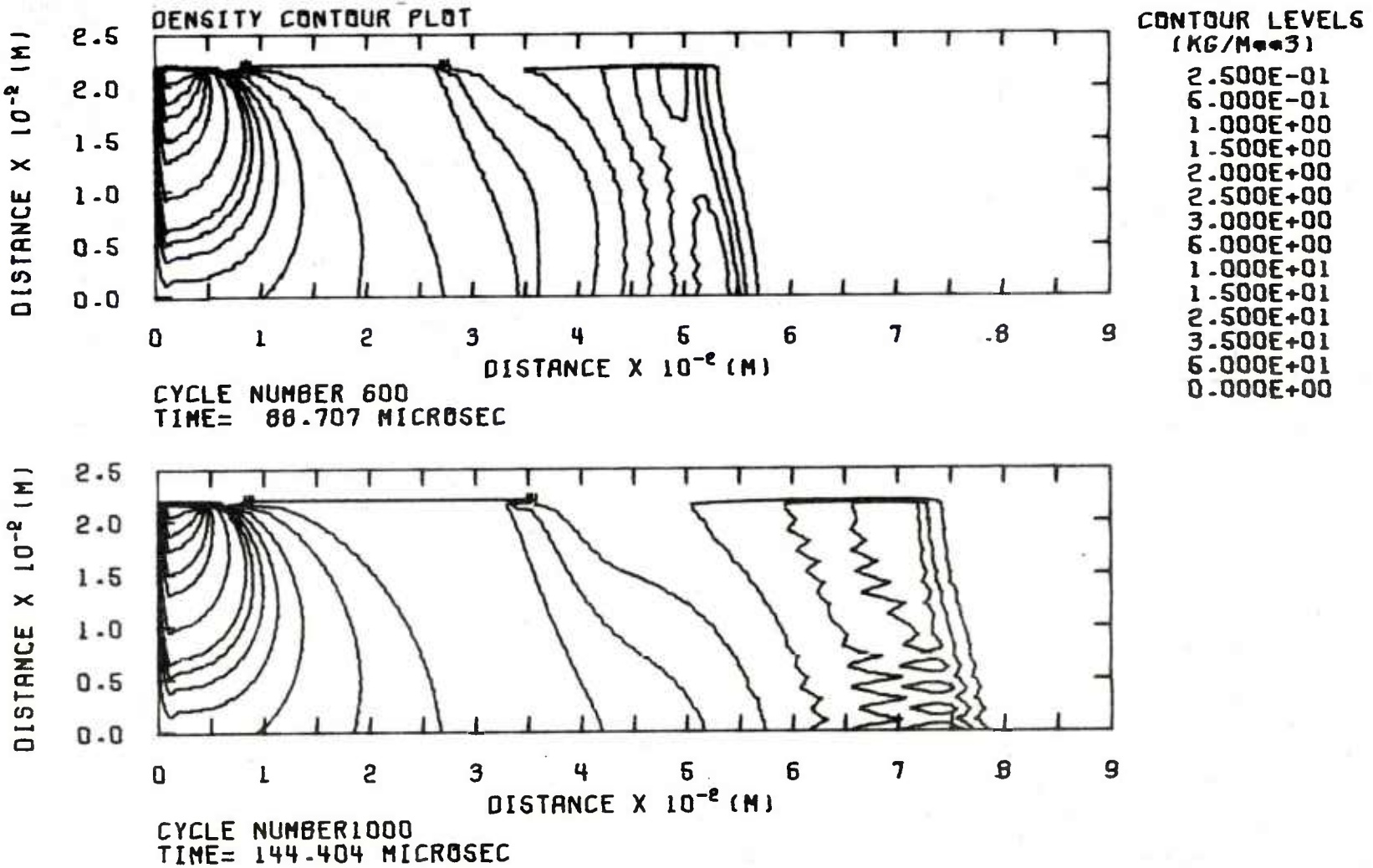

Figure 23. Density contour plots of the primer jet in the stand-off region at t = 88.70 and 144.40 [μs].

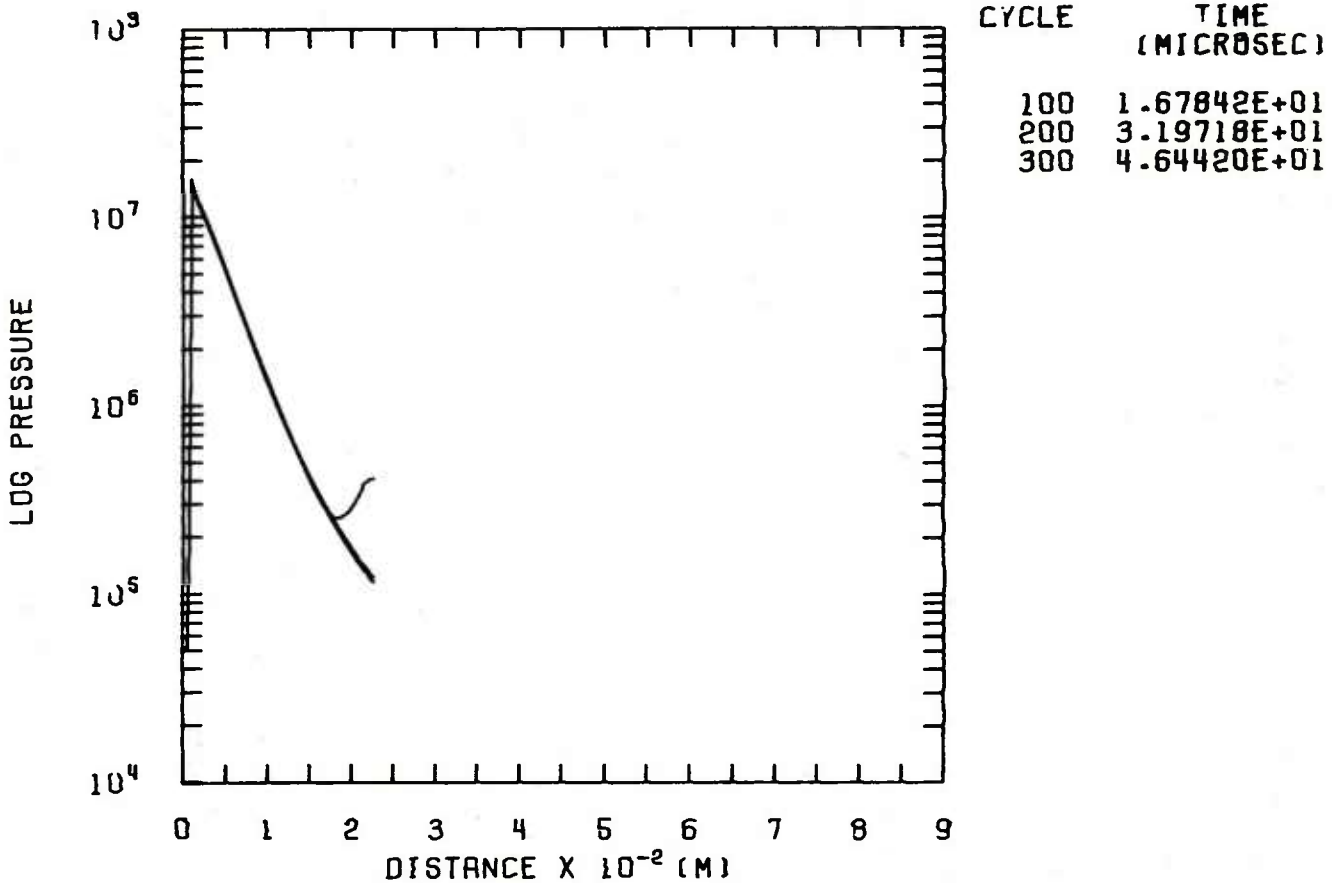

Figure 24. Pressure along the jet axis in the stand-off region at t = 16.78, 31.97 and 46.44 [μs].

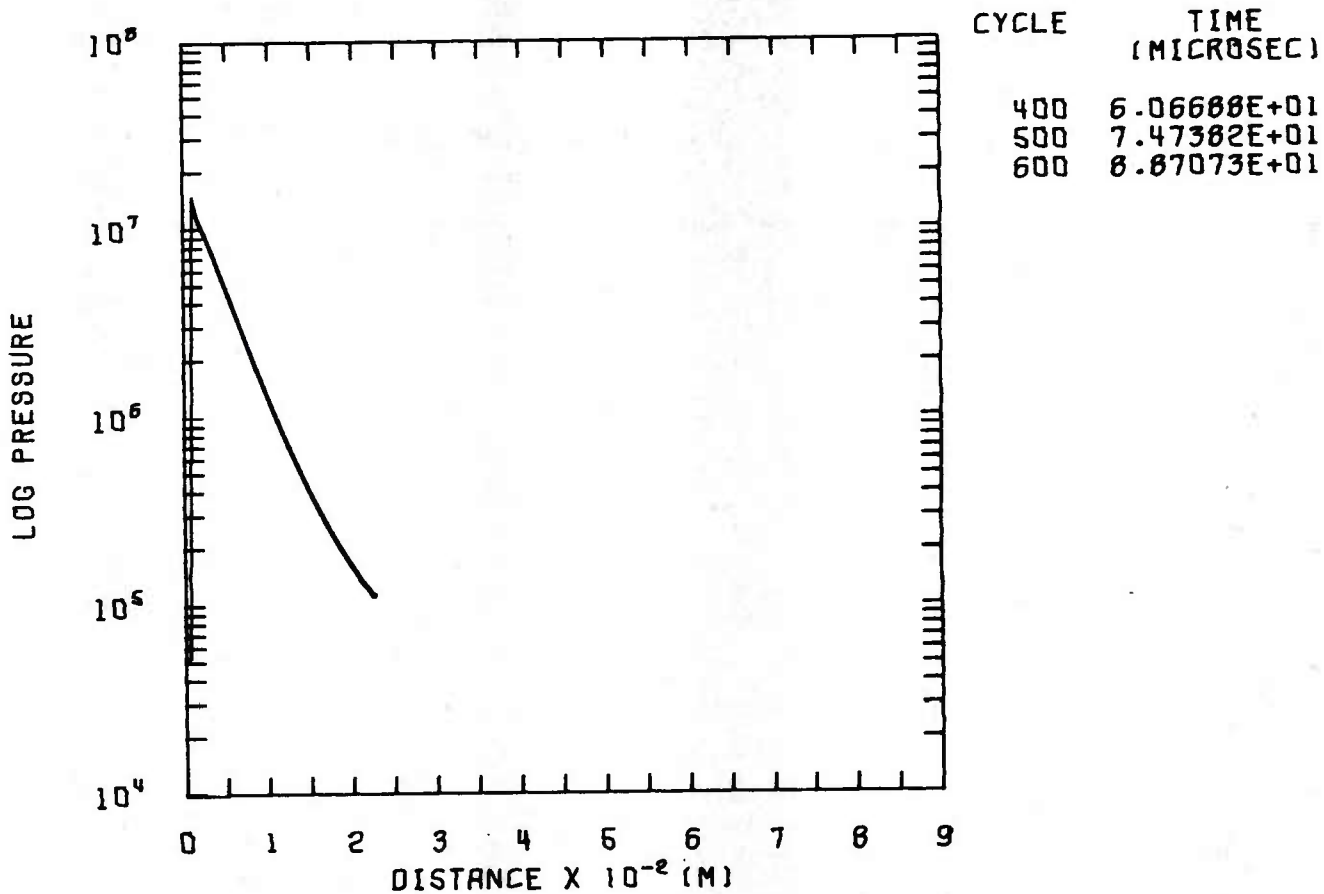

Figure 25. Pressure along the jet axis in the stand-off region at t = 60.66, 74.73 and 88.70 [μs].

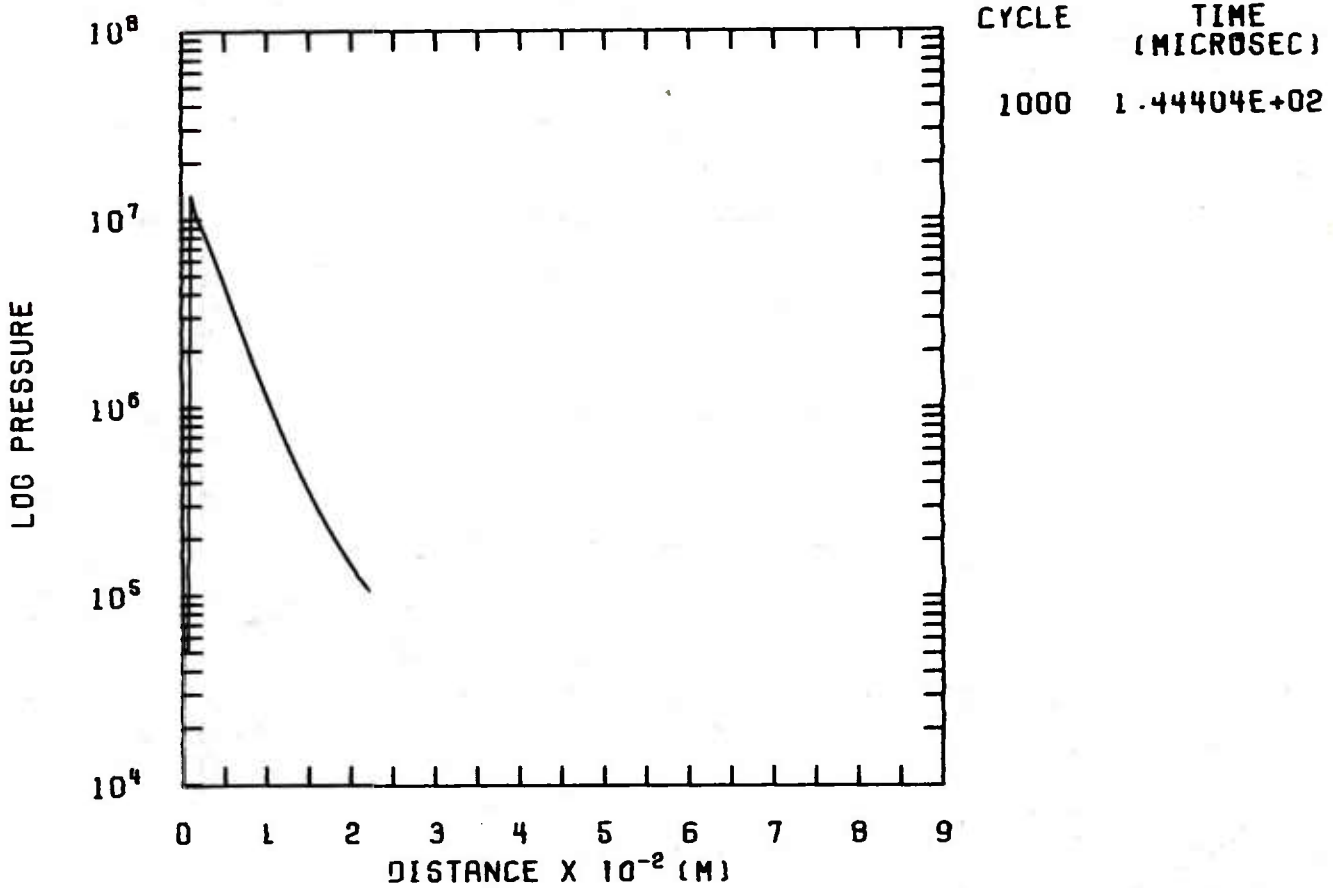

Figure 26. Pressure along the jet axis in the stand-off region at t = 144.40 [μs].

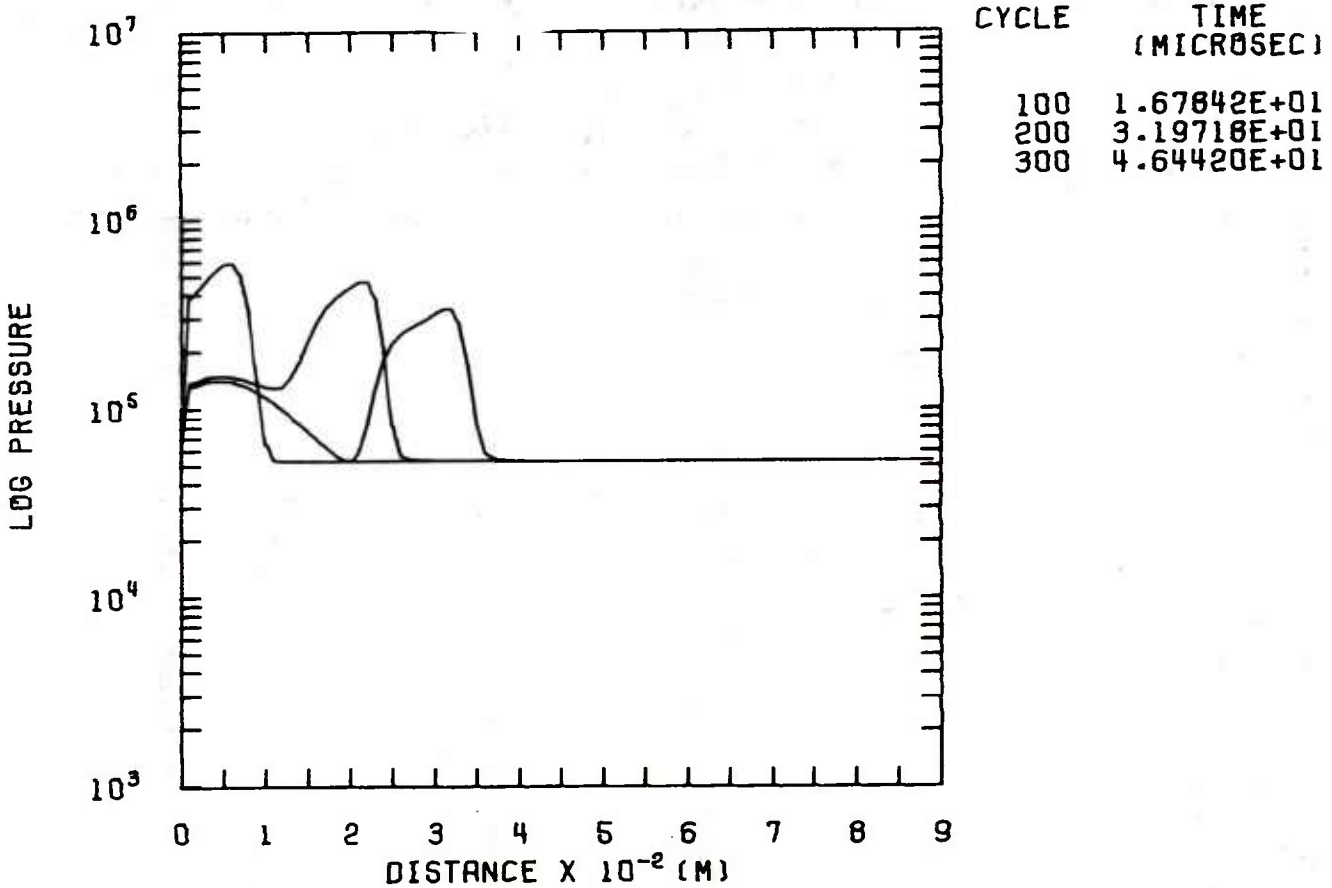

Figure 27. Pressure radially from the jet axis along the propellant bag base at t = 16.78, 31.97 and 46.44 [μs].

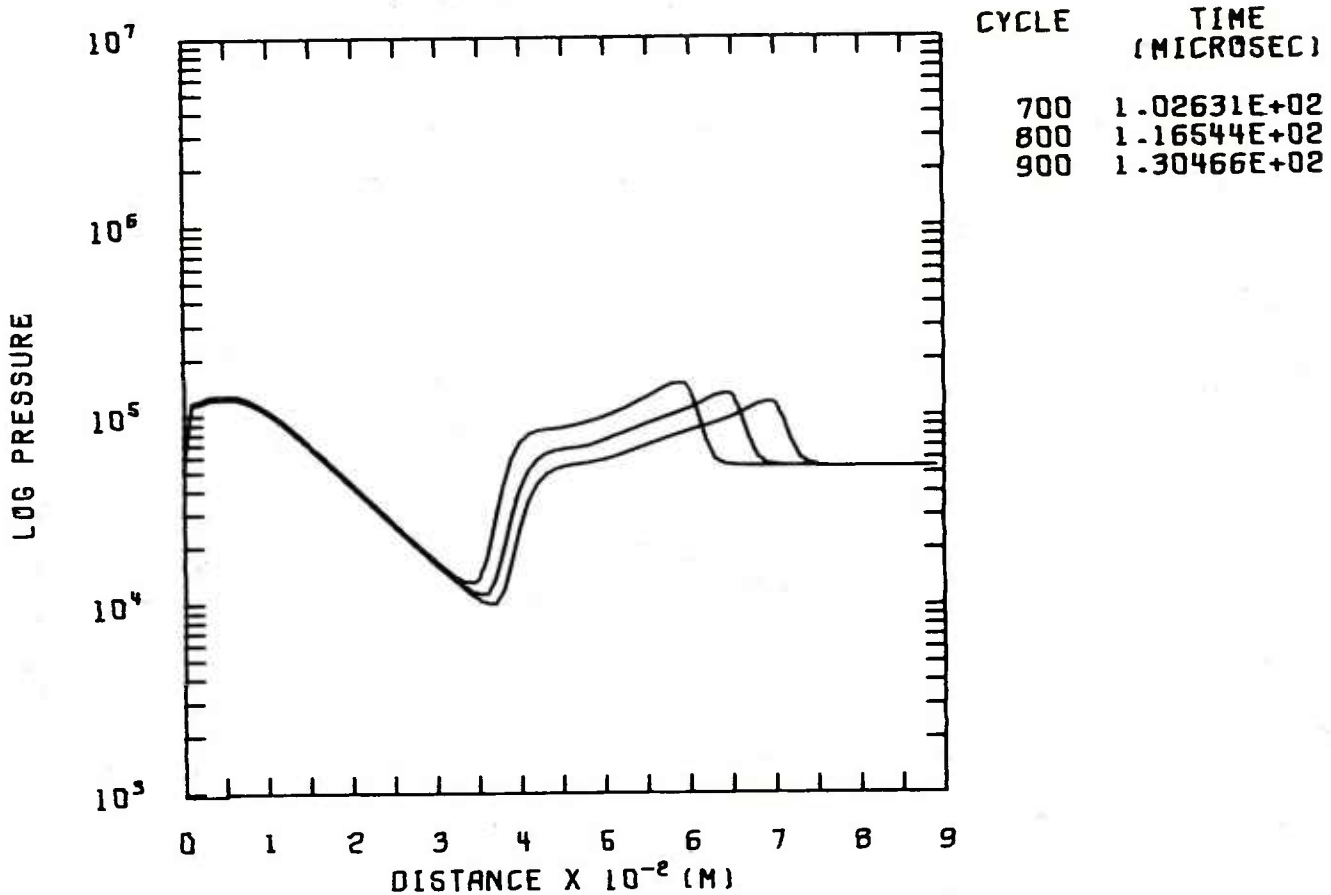

Figure 28. Pressure radially from the jet axis along the propellant bag base at t = 102.63, 116.54 and 130.46 [μs].

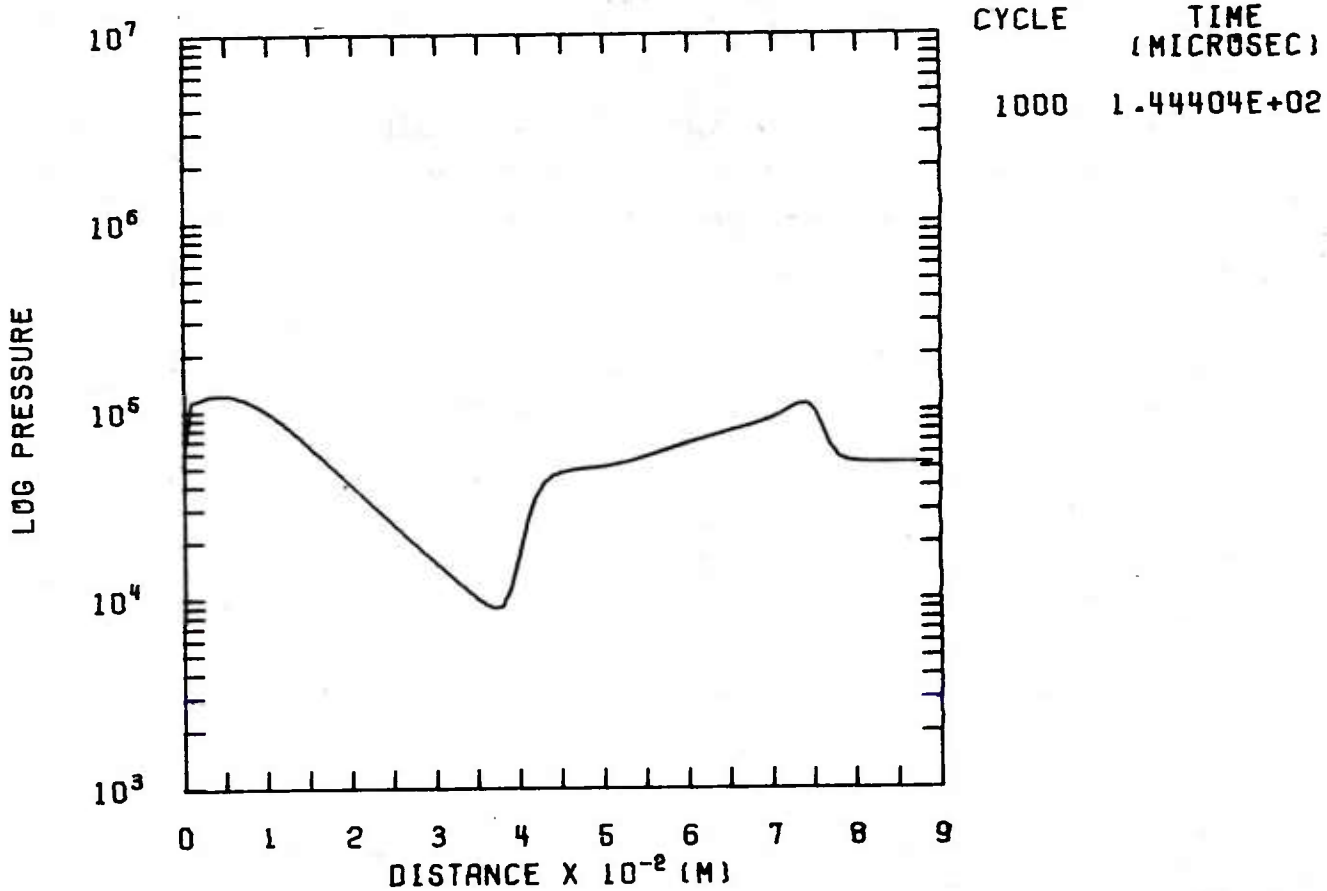

Figure 29. Pressure radially from the jet axis along the propellant bag base at t = 144.40 [μs].

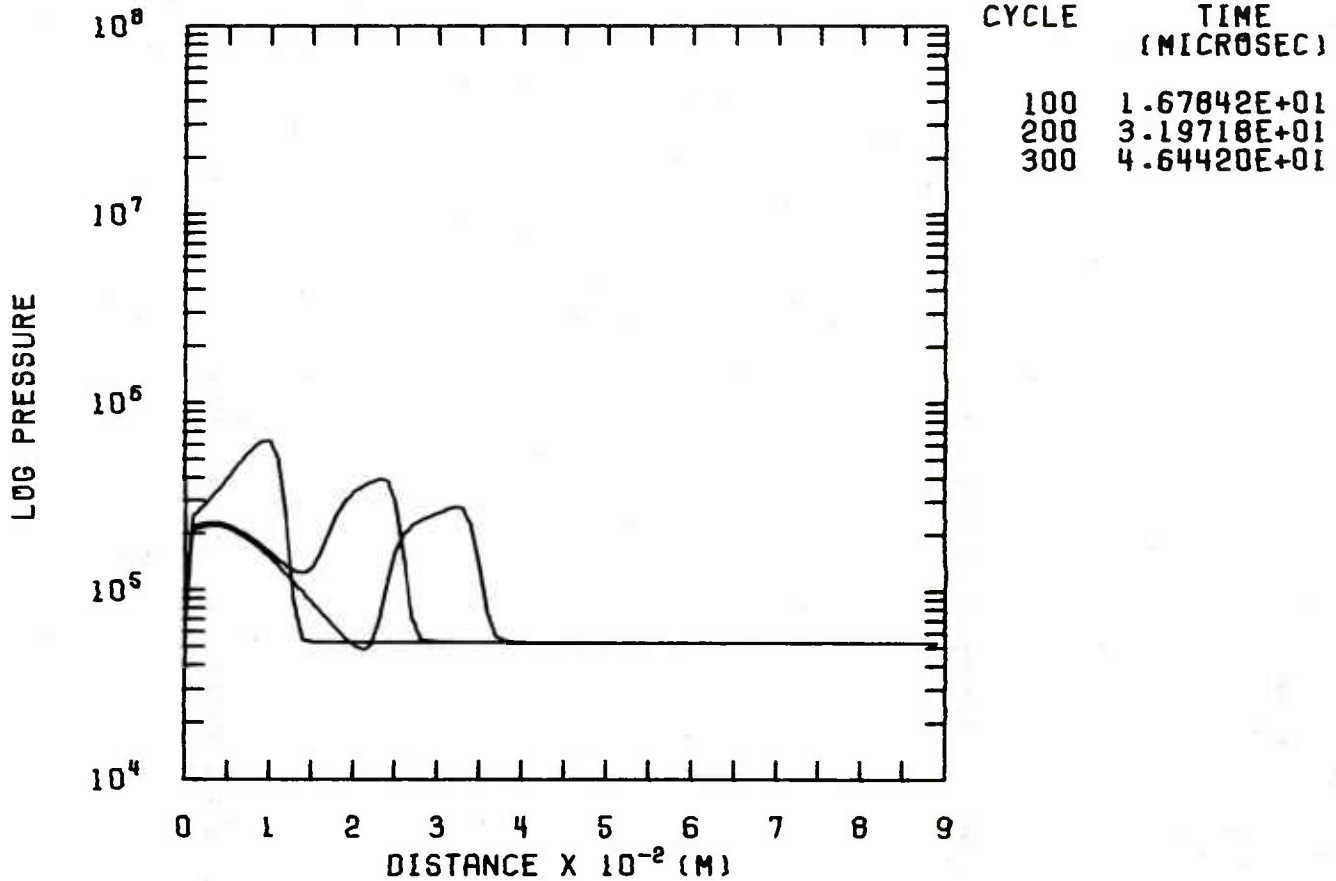

Figure 30. Pressure radially from the jet axis at 4.00 x 10^{-3}[m] from the propellant bag base at t = 16.78, 31.97 and 46.44 [μs].

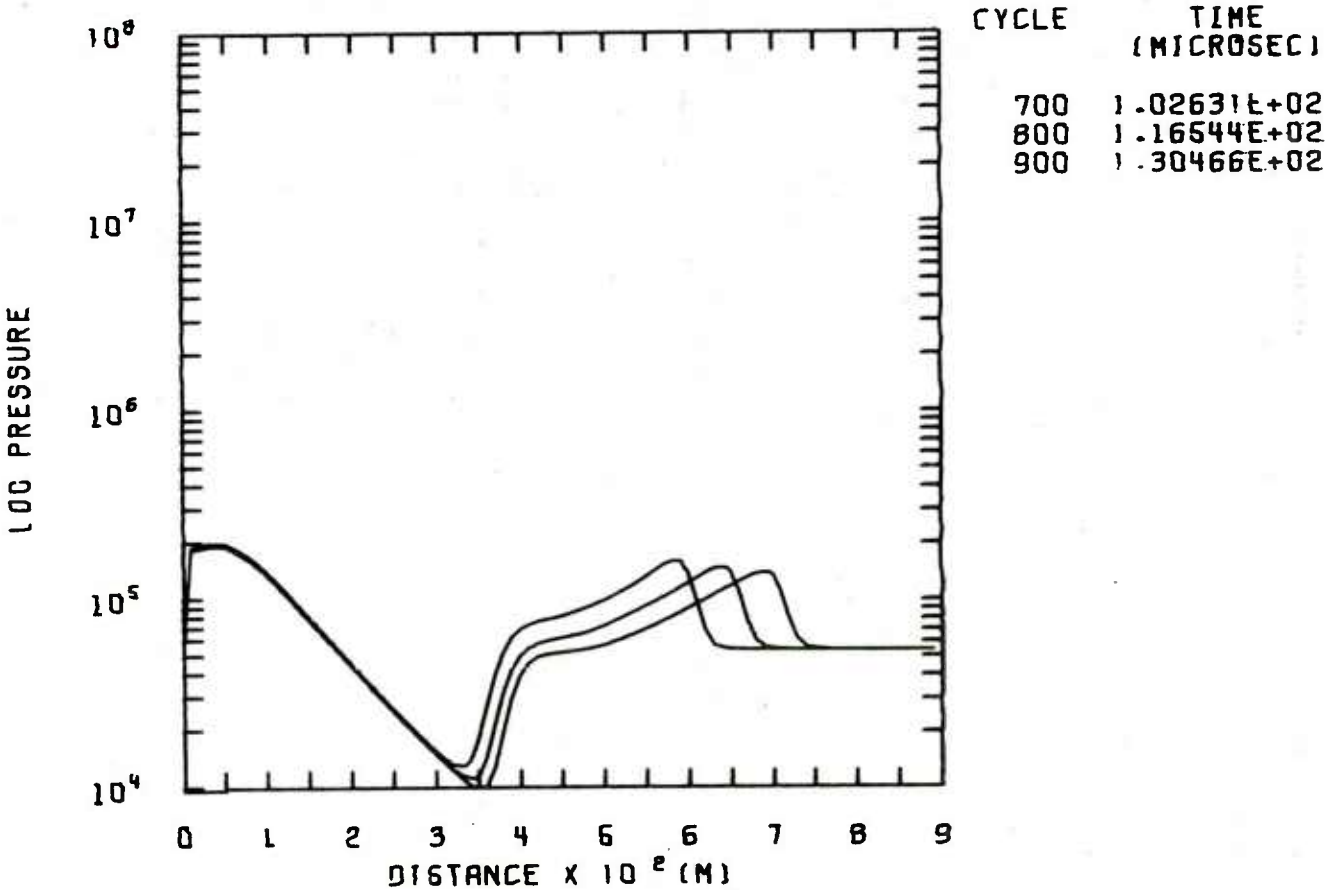

Figure 31. Pressure radially from the jet axis at 4.00 x 10^{-3}[m] from the propellant bag base at t = 102.63, 116.54 and 130.46 [μs].

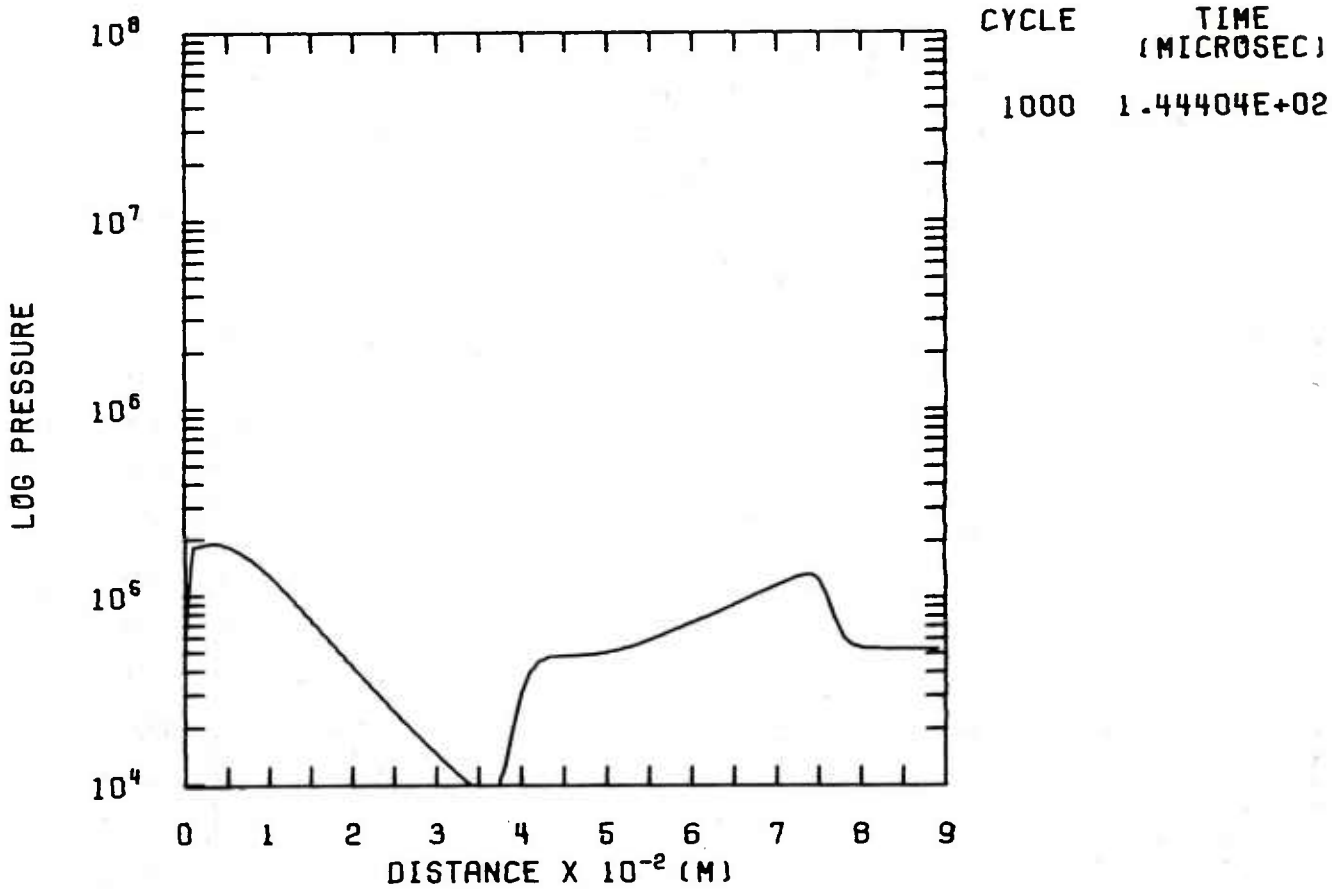

Figure 32. Pressure radially from the jet axis at 4.00 x 10^{-3}[m] from the propellant bag base at t = 144.40 [μs].

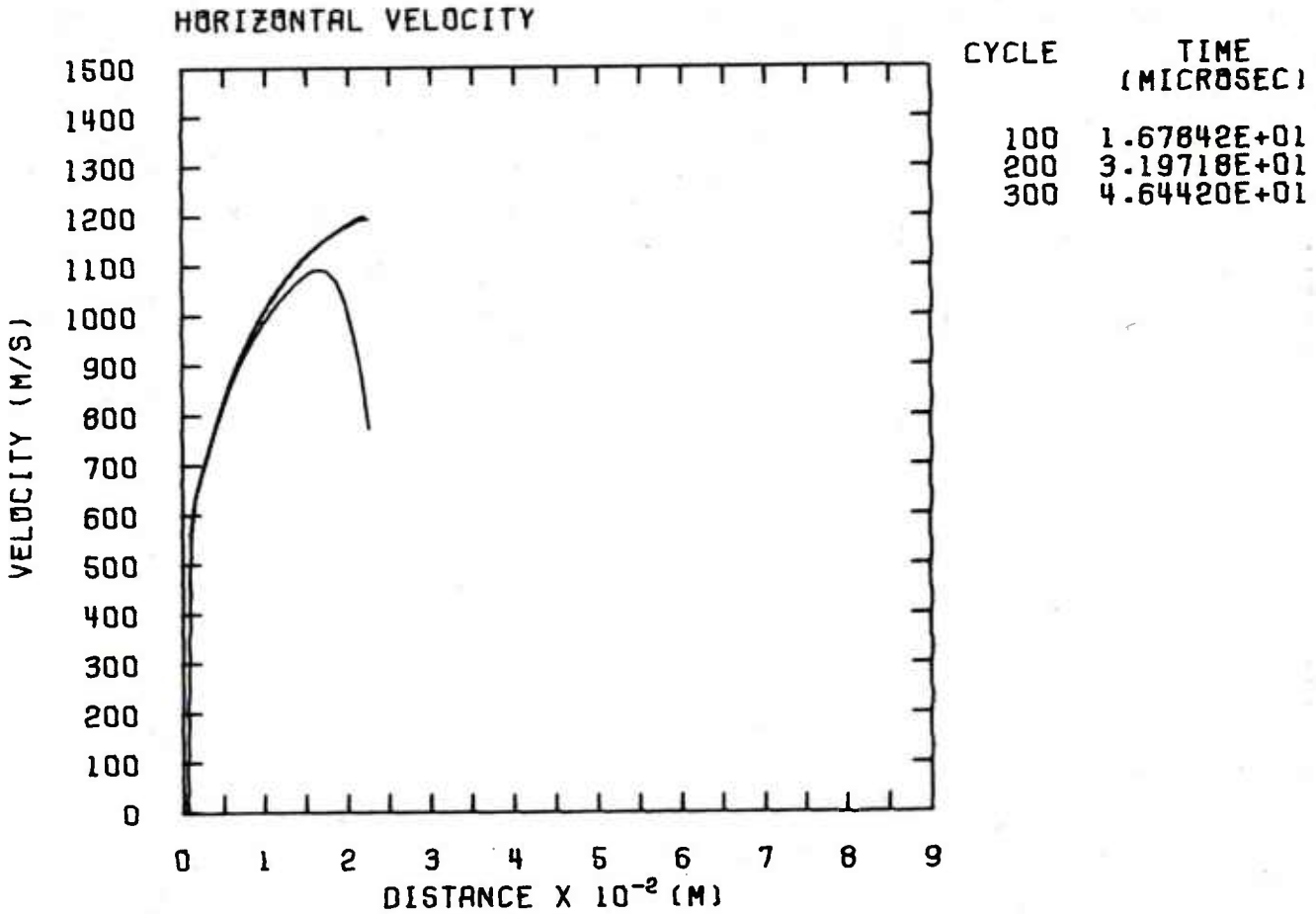

Figure 33. Velocity along the jet axis in the stand-off region at t = 16.78, 31.97 and 46.44 [μs].

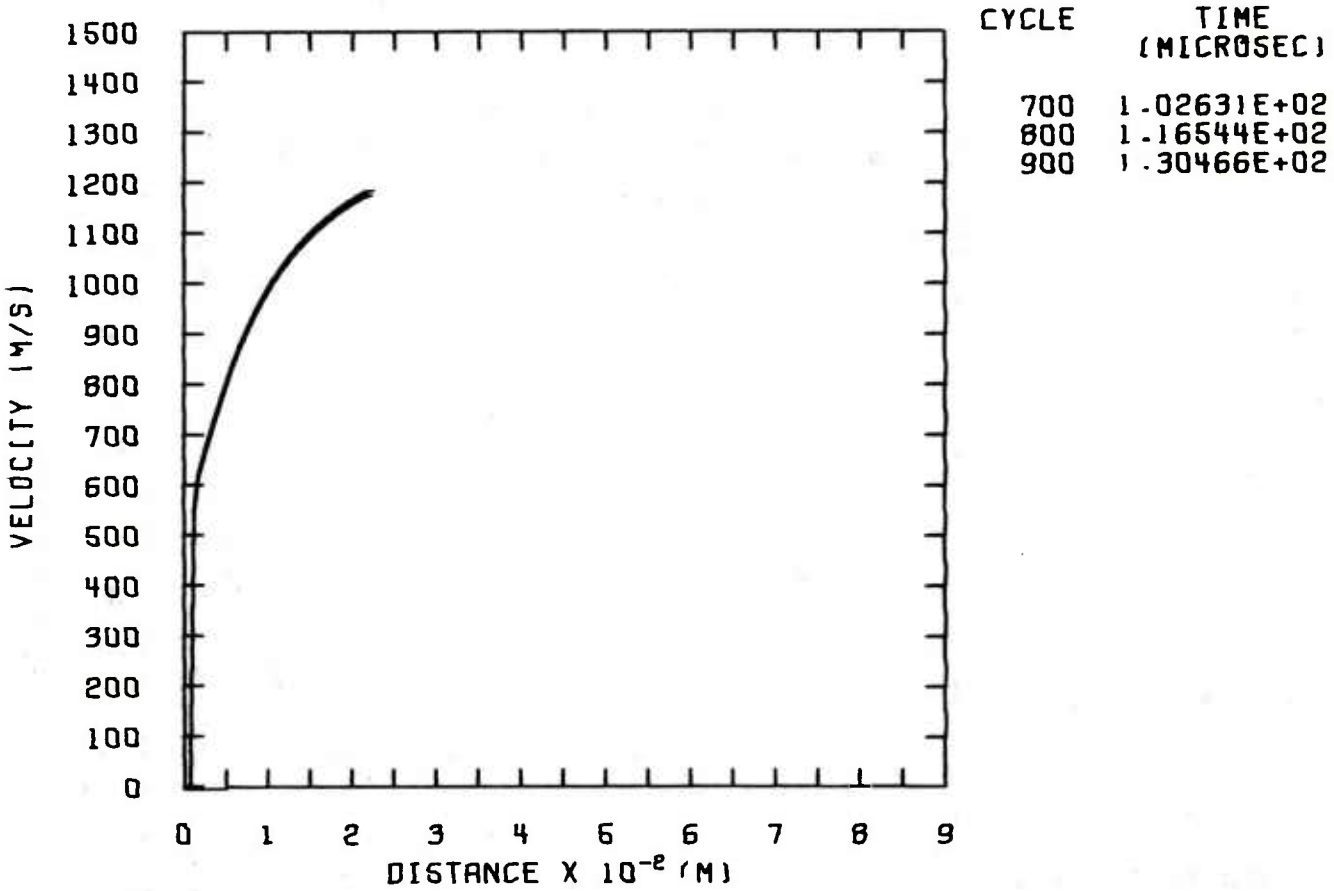

Figure 34. Velocity along the jet axis in the stand-off region at t = 102.63, 116.54 and 130.46 [μs].

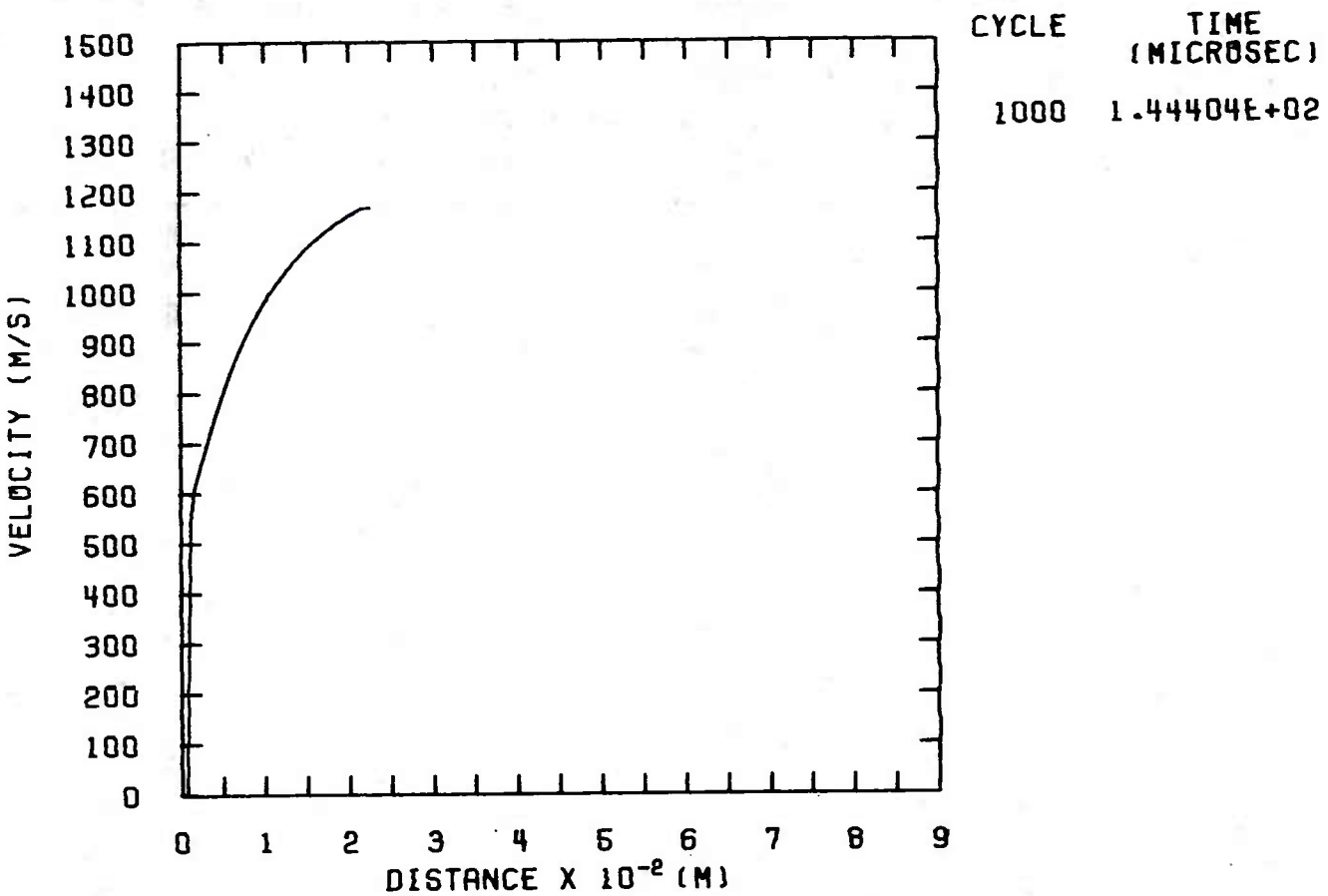

Figure 35. Velocity along the jet axis in the stand-off region at t = 144.40 [μs].

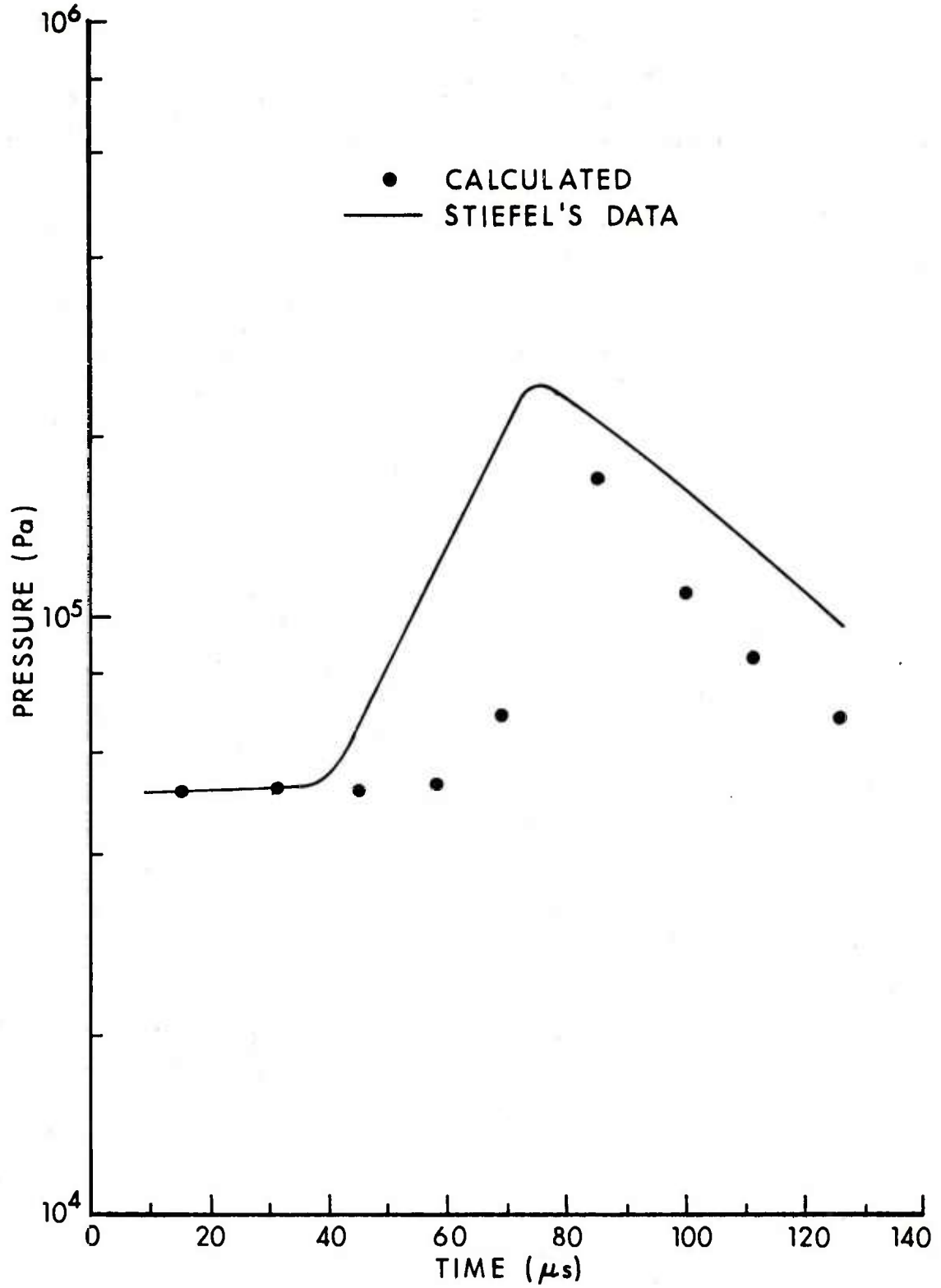

Figure 36. Comparison between calculated and measured pressures at a location 0.0508 [m] from the jet axis at the propellant bag base as a function of time. Stiefel's data is from Reference 9.

LIST OF SYMBOLS

$A(x)$	base area	$[m^2]$
c	specific heat of solid particles	[J/K kmol]
c_p	specific heat at constant pressure	[J/K kmol]
c_v	specific heat at constant volume	[J/K kmol]
F	force per unit mass due to friction	$[m/s^2]$
P	pressure	[Pa]
q	heat generation rate/mass	[J/kg•s]
t	time	[s]
u	axial gas velocity	[m/s]
R	universal gas constant	[J/K kmol]
M	molar mass	[kg/mol]
n	burning rate exponent	
z	surface regression distance	[m]
β	burning rate coefficient	
δ	$\frac{c}{c_p}$	
γ	ratio of specific heats of the gas	
γ_m	ratio of specific heats of the mixture	
ρ	density	$[kg/m^3]$

LIST OF SYMBOLS (cont'd)

η	covolume	$[\frac{m^3}{kg}]$
τ	solid particle temperature	[K]
ϕ	particle mass fraction	

DISTRIBUTION LIST

No. of Copies	Organization
12	Commander Defense Documentation Center ATTN: DDC-TCA Cameron Station Alexandria, VA 22314
1	Commander US Army Materiel Development and Readiness Command ATTN: DRCDMD-ST 5001 Eisenhower Avenue Alexandria, VA 22333
3	Commander US Army Aviation Research and Development Command ATTN: DRSAV-E DRSAV-EQA, CPT Schrage DRCPM-AAH, G. Smith 12th and Spruce Streets St. Louis, MO 63166
1	Director US Army Air Mobility Research and Development Laboratory Ames Research Center Moffett Field, CA 94035
1	Commander US Army Electronics Research and Development Command Technical Support Activity ATTN: DELSD-L Fort Monmouth, NJ 07703
1	Commander US Army Communications Rsch and Development Command ATTN: DRDCO-SGS Fort Monmouth, NJ 07703
6	Commander US Army Missile Research and Development Command ATTN: DRDMI-R DRDMI-RDK Mr. R. Becht (4 cys) Mr. R. Deep Redstone Arsenal, AL 35809
1	Commander US Army Missile Materiel Readiness Command ATTN: DRSMI-AOM Redstone Arsenal, AL 35809
1	Commander US Army Tank Automotive Research & Development Cmd ATTN: DRDTA-UL Warren, MI 48090
3	Commander US Army Armament Materiel Readiness Command ATTN: P. Ehle DRSAR-RDG, J. Blick DRSAR-LEP-L, Tech Lib Rock Island, IL 61299
4	Commander US Army Armament Research and Development Command ATTN: DRDAR-TSS (2 cys) DRDAR-TDS, Mr. Lindner DRDAR-QA, F. Fitzsimmons Dover, NJ 07801
1	Commander US Army Armament Research and Development Command ATTN: DRCPM-AAH (30 mm) Mr. A. Cianciosi Dover, NJ 07801

DISTRIBUTION LIST

No. of Copies	Organization
5	Commander US Army Armament Research and Development Command ATTN: DRDAR-LCA, Mr. A. Loeb DRDAR-LCA-FD Mr. D. Mertz Mr. F. Friedman DRDAR-LCA-FF Mr. S. Wasserman Mr. L. Stiefel Dover, NJ 07801
3	Commander US Army Armament Research and Development Command ATTN: DRDAR-LCE-CI Mr. Lenchitz DRDAR-LCS, S. Hirshman DRDAR-LCU, E. Barrieres Dover, NJ 07801
4	Commander USA Watervliet Arsenal, ARRADCOM ATTN: Tech Lib SARWV-PDR-S, Dr. F.Sautter SARWV-PDR-AMM, Dr. J.Zweig SARWV-RDD-SE, P. A. Alto Watervliet, NY 12189
1	Commander USA Jefferson Proving Ground ATTN: STEJP-TD-D Madison, IN 47250
1	Commander US Army Harry Diamond Labs ATTN: DRXDO-DAB, H. J. Dabis 2800 Powder Mill Road Adelphi, MD 20783
1	Commander US Army Materials and Mechanics Research Center ATTN: DRXMR-ATL Watertown, MA 02172
1	Director US Army TRADOC Systems Analysis Activity ATTN: ATAA-SL, Tech Lib White Sands Missile Range NM 88002
1	Commander US Army Combat Developments Systems Analysis Group Fort Belvoir, VA 22060
2	Commandant US Army Infantry School ATTN: AJIIS-M Fort Benning, GA 31905
1	President US Army Infantry Board Fort Benning, GA 31905
6	Commander US Army Forces Command ATTN: ATIT-RD-MD (4 cys) ATCOM-P (2 cys) Fort McPherson, GA 30330
1	Department of Ordnance US Military Academy ATTN: Assoc Prof West Point, NY 10996
1	Director US Army BMD Advanced Technology Center P.O. Box 1500, West Station Huntsville, AL 35807
1	Commander US Army Ballistic Missile Defense Systems Command P. O. Box 1500 Huntsville, AL 35807

DISTRIBUTION LIST

No. of Copies	Organization
1	Office of Naval Research ATTN: Code 460 Washington, DC 20360
4	Commander Naval Surface Weapons Center ATTN: Code GX, Dr. W. Kemper Mr. F. H. Maille Dr. G. Moore DX-21, Lib Br. Dahlgren, VA 22448
3	Commander Naval Weapons Center ATTN: Code 553, Tech Lib Code 6003 Dr. W. Hazeltine Code 511, Mr. A. Rice China Lake, CA 93555
2	Commander Naval Ordnance Station ATTN: Code FS13A, P. Sewell Code 5235C, A. Horst Indian Head, MD 20640
2	Commandant US Marine Corps ATTN: A04F AX Washington, DC 20380
1	AFWL (DEV) Kirtland AFB, NM 87117
1	ASD/XRA (Stinfo) Wright-Patterson AFB, OH 45433
1	Advanced Technology Labs ATTN: Dr. J. Erdos Merrick & Steward Avenues Westbury, NY 11590
1	Calspan Corporation ATTN: Mr. G. A. Sterbutzel P. O. Box 235 Buffalo, NY 14221
1	Technical Director Colts Firearms Corporation 150 Huyshore Avenue Hartford, CT 14061
1	General Electric Corporation Armaments Division ATTN: Mr. R. Whyte Lakeside Avenue Burlington, VT 05401
1	Paul Gough Associates, Inc. P. O. Box 1614 Portsmouth, NH 03801
1	Winchester-Western Division Olin Corporation New Haven, CT 06504
1	Sandia Laboratories ATTN: Aerodynamics Department Org 9320, R. Maydew Albuquerque, NM 87115
1	University of Mississippi Mechanical Engineering Dept. ATTN: Prof. Ray Wimberly University, MS 38677

Aberdeen Proving Ground

Dir, USAMSAA
ATTN: Dr. J. Sperrazza
Mr. Simmons
Mr. Clifford
Dir, USAMTD
ATTN: Small Arms Br
Cdr, USATECOM
ATTN: DRSTE-SG-H